

Supporting Information

Four Strategies towards Customized Rainbow/White Light Emission from a Series of Organic Charge-Transfer Cocrystals and Their Heterostructures

Yifu Chen,^{1,2} Bo Jing,^{1,2} Jie Li,^{1,2} Junbo Gong^{1,2,*}

¹ State Key Laboratory of Chemical Engineering, School of Chemical Engineering and Technology, Tianjin University, Weijin Road 92, Tianjin 300072, China.

² Collaborative Innovation Center of Chemical Science and Engineering, Weijin Road 92, Tianjin 300072, China.

*To whom correspondence should be sent: junbo_gong@tju.edu.cn.

Mater. Chem. Front.

Author Contributions:

Y.C. conceptualized the project, directed the study, determined the methods, performed the experiments, analyzed and discussed the results, wrote the manuscript, and drew the figures. Under the supervision of Y.C., B.J. and J.L. helped organized the supporting information. J.G. acquired funding for the whole study. All authors commented on the manuscript.

Supplement Files Involve:

- **A PDF File** (Supplementary Text with Experimental Information, Figures and Tables)
- **Crystallographic Data**
 - DBT-TCNB-b, CCDC 1967489 (Cif_1.cif)
 - DBF-TCNB-b, CCDC 1967486 (Cif_2.cif)
 - DBS-TCNB-b, CCDC 2056561 (Cif_3.cif)
 - PHT-TCNB-b, CCDC 2013883 (Cif_4.cif)
 - CBZ-TCNB-b, CCDC 1967476 (Cif_5.cif)
 - BPE-TCNB-hb, CCDC 2017789 (Cif_6.cif)
 - PHT-TCNB-hb, CCDC 1967483 (Cif_7.cif)
 - CBZ-TCNB-hb, CCDC 1967490 (Cif_8.cif)

List of Contents

Chemicals and Instruments	S-3
Detailed Experimental Procedures	S-3
Crystallographic Information	S-8
Photoluminescence Characterizations	S-18
Density Functional Theory Computations	S-31
Jabłoński Diagram of the Charge-Transfer Complex	S-31
The Growth Process of ABA/AB-Type Heterostructures	S-32
The Conceptual Optical Logic Gate Based on the ABC-Type Heterostructures	S-32
References	S-34

Chemicals and Instruments

All reagents were commercially available and used as received without further purification. 1,2-di(4-pyridyl)ethylene (BPE, 98%) and 1,2,4,5-tetracyanobenzene (TCNB, 97%) were purchased from Heowns Chemical. Naphthalene (NAP, 98%) and dibenzothiophene (DBT, 99%) were purchased from Aladdin Chemical. Dibenzofuran (DBF, 98%) was purchased from D&B Biological. Phenanthrene (PHT, 95%) was purchased from Tianjin Guangfu Fine Chemical Research Institute. Dibenzoselenophene (DBS, 95%) was purchased from Aslee Chemical. Anthracene (ANT, 99.5%) was purchased from Macklin Chemical. Carbazole (CBZ, 99%) was purchased from J&K Chemical. N,N-dimethylformamide (DMF, 99.5%) and acetonitrile (MeCN, 99.5%) were purchased from Tianjin Kemiou Chemical. All water used in our experiments is distilled water.

Single crystal structures of organic charge-transfer cocrystals were obtained on an X-ray diffractometer (Rigaku MicroMax-007). The X-ray crystallographic diffraction data were collected using a Rigaku D/Max 2500. The microphotographs of crystals were taken using the polarizing optical microscope (Nikon DS-Fi3). A 365 nm monochromatic ultraviolet (UV) light emitted via a HTLD-4 II UVLED (Shenzhen Zhijun Optoelectronic Technology Corporation, $\Phi=10$ mm, DC 12-32 V) was used as excitation light source. The absorbance spectra of crystals were measured on UV-2700 spectrophotometer (Shimadzu Instruments). The luminescent spectra of crystals and solutions were measured on an F-4600 fluorescence spectrophotometer (Hitachi-High Technologies). The luminescent quantum yield and lifetime of the as-prepared crystals were measured using a FLS 1000 (Edinburgh Instruments) configured with an integrated sphere. Weighing and gravimetric analysis were carried out on a five digit balance, up to 0.01 mg (Mettler-Toledo, ML204T/02). A micro-solution of 0.01 mL was taken by a 10- μ L trace syringe (Hamilton, P/N: 7653-01) during the preparation of charge-transfer solid solution. The 365 nm light-emitting diodes chip (VQ-P003UVA, 365-370 nm) used to prepare the white light-emitting diodes was purchased from Shenzhen vanq Technology Co. A ZF-7A handheld UV Lamp from Shanghai Gucun Optic Instrument Factory is also used.

Detailed Experimental Procedures

1. Preparation of a series of charge-transfer crystals

BPE-TCNB-b and BPE-TCNB-hb crystals: BPE (18.6 mg, 0.1 mmol) and TCNB (18.4 mg, 0.1 mmol) were added into 20 mL MeCN, dissolved well. After quick solvent evaporation for 2-3 days, the millimeter-scale plate-like BPE-TCNB-b crystals were obtained. BPE (18.6 mg, 0.1 mmol) and TCNB (18.4 mg, 0.1 mmol) were added into 10 mL DMF, dissolved well. After slow solvent evaporation for 7-10 days, the millimeter-scale rod-like BPE-TCNB-hb crystals were obtained.

PHT-TCNB-b and PHT-TCNB-hb crystals: PHT (17.8 mg, 0.1 mmol) and TCNB (18.4 mg, 0.1 mmol) were added into 20 mL MeCN, dissolved well. After quick solvent evaporation for 2-3 days, the millimeter-scale rod-like PHT-TCNB-b crystals were obtained. PHT (17.8 mg, 0.1 mmol) and TCNB (18.4 mg, 0.1

mmol) were added into 10 mL DMF, dissolved well. After slow solvent evaporation for 7-10 days, the millimeter-scale rod-like PHT-TCNB-hb crystals were obtained.

CBZ-TCNB-b and CBZ-TCNB-hb crystals: CBZ (16.9 mg, 0.1 mmol) and TCNB (18.4 mg, 0.1 mmol) were added into 20 mL MeCN, dissolved well. After quick solvent evaporation for 2-3 days, the millimeter-scale rod-like CBZ-TCNB-b crystals were obtained. CBZ (16.9 mg, 0.1 mmol) and TCNB (18.4 mg, 0.1 mmol) were added into 10 mL DMF, dissolved well. After slow solvent evaporation for 7-10 days, the millimeter-scale rod-like CBZ-TCNB-hb crystals were obtained.

NAP-TCNB-b, DBT-TCNB-b, DBF-TCNB-b, DBS-TCNB-b, ANT-TCNB-b crystals: Rod-like NAP-TCNB-b crystals, rod-like DBT-TCNB-b crystals, rod-like DBF-TCNB-b crystals, rod-like DBS-TCNB-b crystals, rod-like ANT-TCNB-b crystals were obtained from quick solvent evaporation for 2-3 days from 20 mL MeCN solution of donors (0.005 mol/L) and TCNB (0.005 mol/L).

2. X-ray diffraction for the crystal face identification of all charge-transfer crystals: A regular millimeter-scale charge-transfer crystal was placed with the main crystal face upward on the center of a sample holder for X-ray diffraction. The diffraction result was compared with the simulated crystallographic diffraction pattern based on its corresponding single-crystal structure to identify the main crystal face of this charge-transfer crystal.

3. Preparation of a series of charge-transfer complexes in solutions

Charge-transfer complexes in MeCN/H₂O solution: 0.1 mL MeCN solution of donor and TCNB (0.005 mol/L donor and 0.005 mol/L TCNB) was added into the 4 mL glass bottle, then dilute it with 4 mL pure water.

Charge-transfer complexes in DMF/H₂O solution: 0.05 mL DMF solution of donor and TCNB (0.01 mol/L donor and 0.01 mol/L TCNB) was added into the 4 mL glass bottle, and then dilute it with 4 mL pure water.

4. Preparation of the white light-emitting charge-transfer solid solution

It needs three steps to prepare the charge-transfer solid solution.

Step 1, Prepare a solution of ANT-TCNB: ANT (17.8 mg, 0.1 mmol) and TCNB (18.4 mg, 0.1 mmol) were added into 20 mL MeCN, dissolved well.

Step 2, Prepare a solution of NAP-TCNB: NAP (12.8 mg, 0.1 mmol) and TCNB (18.4 mg, 0.1 mmol) were added into 20 mL MeCN, dissolved well.

Step 3, Prepare the solid solution: We use a trace syringe to take 0.01 mL solution of ANT-TCNB and add it to the 20 mL solution of NAP-TCNB to prepare a mixing solution. Finally, 0.1 mL mixing solution was added

into the 4 mL glass bottle, then dilute with 4 mL pure water. The appending proportion of NAP-TCNB:ANT-TCNB is about 1:0.05%, result in a $\text{NAP}_{0.9995}\text{ANT}_{0.0005}\text{TCNB}$. Single crystals were obtained upon evaporation and observed under the microscope.

Note: The proportion of NAP and ANT in $\text{NAP}_{0.9995}\text{ANT}_{0.0005}\text{TCNB}$ solid solution is estimated by the proportion of feed ratio. We have tried to characterize the content of NAP, ANT and TCNB in the as-prepared solid solution by nuclear magnetic resonance (NMR) but can not. The reasons are as follows: 1) The hydrogen atoms of NAP and ANT have similar chemical shifts due to their similar aromatic hydrocarbon structure without substituents, thus can not be indentified by $^1\text{H-NMR}$. 2) Technically, the composition of the mixture cannot be determined by $^{13}\text{C-NMR}$.

5. Preparation of white light-emitting diodes

The white light-emitting diodes devices were fabricated with a 365 nm light-emitting diodes chip and white light-emitting charge-transfer solid solution $\text{NAP}_{0.9995}\text{ANT}_{0.0005}\text{TCNB}$ crystals. The charge-transfer solid solution $\text{NAP}_{0.9995}\text{ANT}_{0.0005}\text{TCNB}$ crystals were added into organic silica gel in a certain proportion, then mixed thoroughly and coated on the 365 nm LED chip. After drying at 100 °C for 12 h, the white light-emitting diodes were obtained.

6. Preparation of a series of multiblock heterostructures single crystals

ABA-type triblock heterostructures crystals: In a typical ABA-type triblock heterostructure preparation experiment, the first step is preparing the seeds. Take GOG triblock heterostructure for example, first, 0.05 mL saturated MeCN solution of ANT-TCNB was dropped on the glass plate, then the ANT-TCNB-b seeds (O) crystallized during solvent evaporation. The secondary growth solution was DBT-TCNB (G) saturated MeCN solution. We use an injector to aspirate some and rinse the ANT-TCNB-b crystals (O) for at least three times. After rinsing, a drop of saturated MeCN solution of DBT-TCNB is added on the seeds of ANT-TCNB-b (O), then GOG triblock heterostructures were obtained during solvent evaporation. Under 365 nm UV light, the resultant triblock heterostructures display green-orange-green luminescence. Other ABA-type triblock heterostructures were fabricated following the similar method.

ABCBA-type pentablock heterostructures crystals: In a typical ABCBA-type pentablock heterostructure preparation experiment, take BGOGB pentablock heterostructure for example, with a similar method to the preparation of ABA-type, we use GOG as seeds, the saturated MeCN solution of NAP-TCNB (B) as secondary growth solution to prepare BGOGB pentablock heterostructure.

AB-type diblock heterostructures crystals: In a typical AB-type diblock heterostructure preparation experiment, take OG diblock heterostructure for example, 0.05 mL saturated MeCN solution of ANT-TCNB was dropped onto a glass plate, then the ANT-TCNB seeds (O) were crystallized during solvent evaporation. Apply a small amount of vaseline on one side of the ANT-TCNB seed crystals with the tip of a needle. Then drop 0.05 mL saturated MeCN solution of DBT-TCNB (G) on the seeds of ANT-TCNB (O). When the solvent evaporated totally, OG diblock crystals were obtained.

ABC/ABCD-type triblock/tetrablock heterostructures crystals: In a typical ABC-type triblock heterostructure preparation experiment, take OGB triblock heterostructure for example, with a similar method to the preparation of AB-type, diblock OG crystals were served as seeds to epitaxial grow triblock heterostructure, the saturated MeCN solution for NAP-TCNB (B) as secondary growth solution to prepare OGB triblock heterostructure. When the solvent evaporated totally, triblock OGB triblock heterostructure crystals were obtained. Other ABCD-type tetrablock heterostructures were fabricated following the similar method of preparing ABC-type. In the preparation experiments of AB-type biblock, ABC-type triblock and ABCD-type tetrablock, vaseline needs to be applied only once at the original seeds, subsequent epitaxial growth is automatically on the free end.

Note: A simpler method for preparing AB-type biblock, ABC-type triblock and ABCD-type tetrablock heterostructure is stated as below. We put a thin layer of vaseline on the inner wall and bottom of a glass bottle. Then we use this glass bottle to prepare seeds. Following more than three times rinse and refilling with the secondary growth solution, and after the solvent evaporation, the AB-type biblock heterostructure will be found next to the inner wall and bottom of the glass bottle. Other ABC-type triblock and ABCD-type tetrablock heterostructure were fabricated following the similar method of preparing AB-type biblock heterostructure.

Note: The "rinse" step plays two key roles during the preparation of heterostructures: (1) keep the seeds wet and (2) refresh the original solution with secondary growth solution on the crystal surface.

7. Measurement of the absorbance spectra

The absorbance spectra of crystals were measured. A customized sample holder (similar to the glass holder for crystallographic testing) was tight filled with crystals for test, with a quartz glass covered. We use this tool to directly measure the ultraviolet-visible diffuse reflection spectra with the quartz glass facing integrating sphere. And the absorbance spectra were calculated from the ultraviolet-visible diffuse reflection spectra.

8. Measurement of the photoluminescence spectra

The photoluminescence spectra of charge-transfer cocrystals were measured in a customized grooved (1 mm deep), high-transparency quartz plate with another high-transparency quartz plate covered, using a FLS 1000 (Edinburgh Instruments). The photoluminescence spectra of the liquid samples are using a four-way quartz cuvette for measurement of liquid luminescence spectra using an F-4600 fluorescence spectrophotometer (Hitachi-High Technologies).

9. Absolute luminescence quantum yields (Φ_{PL})

The luminescent quantum yields (Φ_{PL}) of the as-prepared charge-transfer crystals were measured at room temperature with the excitation wavelength set as 300 nm and the luminescence range was set as 300 nm to 800 nm.

10. Measurement of the photoluminescence anisotropy

The photoluminescence anisotropy properties of the charge-transfer single crystals were measured by our reformed F-4600 fluorescence spectrophotometer as illustrated in Figure S1. Because our fluorescence spectrometer is unable to achieve photoluminescence anisotropy measurement, we fixed the specialized polarizer (with a knob) behind the incident light source. The polarization angle can be adjusted by the knob, and the angle range is 0-360°. The fluorescence spectrum of the crystal was measured every 15° rotation. The crystals are placed horizontally and parallel in one direction. The detector is used to measure the luminescence polarization spectrum of all the charge-transfer cocrystals.

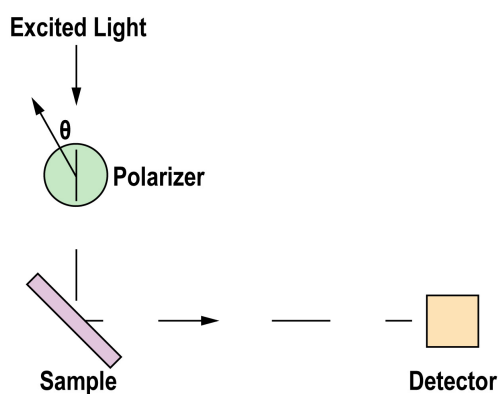


Figure S1. Schematic representations of the experimental setup for photoluminescence anisotropy characterization.

Crystallographic Information

Table S1. Single crystal structure information of a series of organic charge-transfer cocrystals

	CCDC	<i>a</i> /Å	<i>b</i> /Å	<i>c</i> /Å	<i>α</i> /°	<i>β</i> /°	<i>γ</i> /°	<i>V</i> /Å ³
BPE-TCNB-b	1405953	6.875(5)	7.114(5)	10.228(9)	77.49(4)	78.61(4)	75.69(4)	467.70
BPE-TCNB-hb	2017789*	21.784	6.102	14.17	90	104.831	90	1820.85
NAP-TCNB-b	1216897	9.337(3)	12.554(6)	6.738(2)	90	107.40(2)	90	753.66
DBT-TCNB-b	1967489*	7.183	7.803	7.952	73.00	85.67(3)	88.65(3)	425.06
DBF-TCNB-b	1967486*	7.249	7.801	7.856	73.68	81.08	84.74	420.68
DBS-TCNB-b	2056561*	9.354	12.732	14.295	90	92.816	90	1700.43
PHT-TCNB-b	2013883*	9.422	13.085	7.261	90	92.95	90	894.04
PHT-TCNB-hb	1967483*	7.223	7.935	30.653	90	91.50	90	1756.28
ANT-TCNB-b	1103080	9.505(1)	12.748(2)	7.417(2)	90	92.45(2)	90	897.89
CBZ-TCNB-b	1967476*	9.466	12.597	7.143	90	94.21	90	849.426
CBZ-TCNB-hb	1967490*	24.906	7.217	9.291	90	90	90	1669.91

*CCDC number deposited by us. The structures could be downloaded free of charge from the Cambridge Crystallographic Data Centre (www.ccdc.cam.ac.uk/).

Packing mode of the eight kinds of brick-packing charge-transfer cocrystals

Note: All TCNB molecules in charge-transfer cocrystals are represented in purple color, and the donors are represented by different colors.

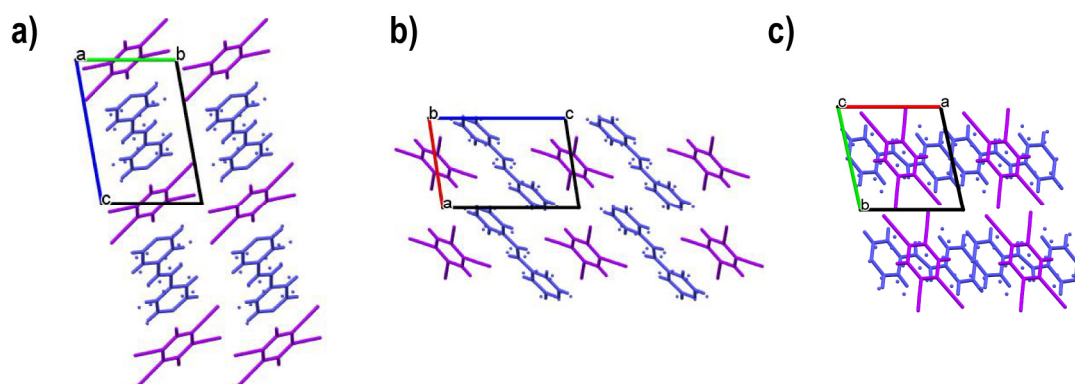


Figure S2. Packing mode of BPE-TCNB-b charge-transfer cocrystal. View along a axis (a), along b axis (b), along c axis (c).

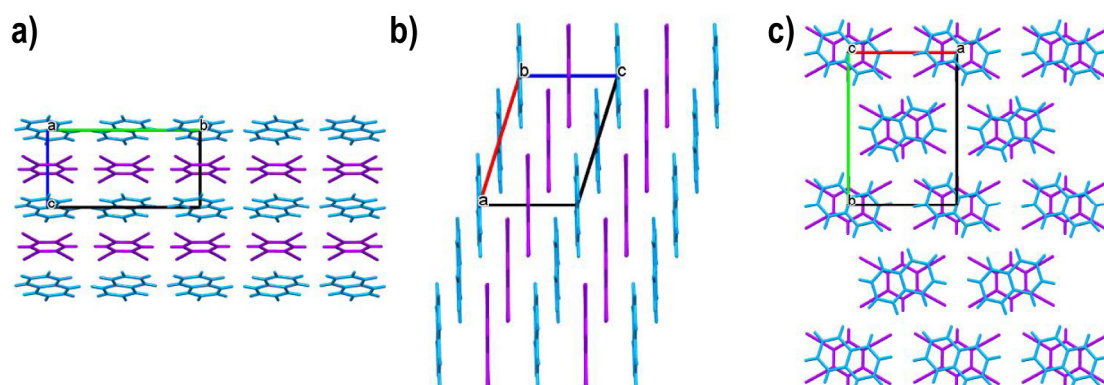


Figure S3. Packing mode of NAP-TCNB-b charge-transfer cocrystal. View along a axis (a), along b axis (b), along c axis (c).

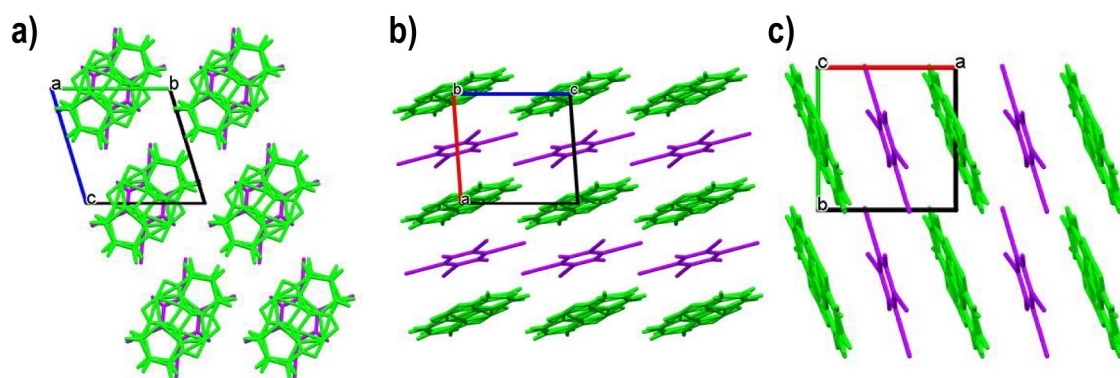


Figure S4. Packing mode of DBT-TCNB-b charge-transfer cocrystal. View along a axis (a), along b axis (b), along c axis (c).

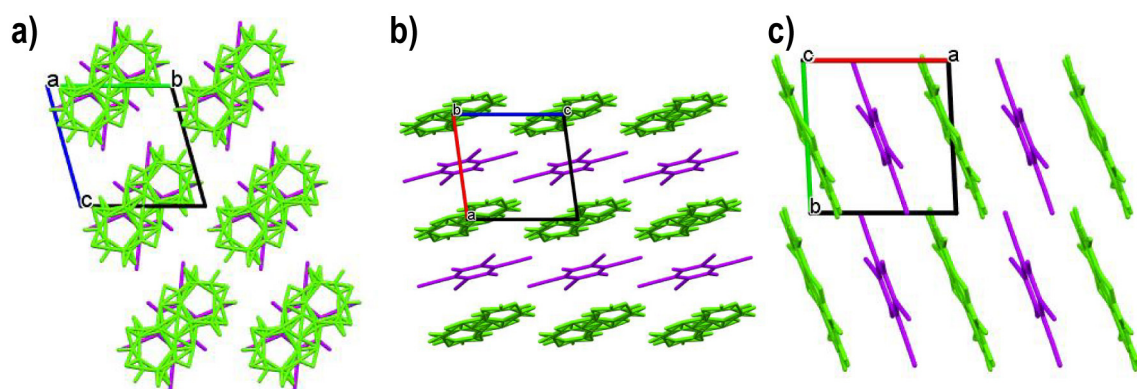


Figure S5. Packing mode of DBF-TCNB-b charge-transfer cocrystal. View along a axis (a), along b axis (b), along c axis (c).

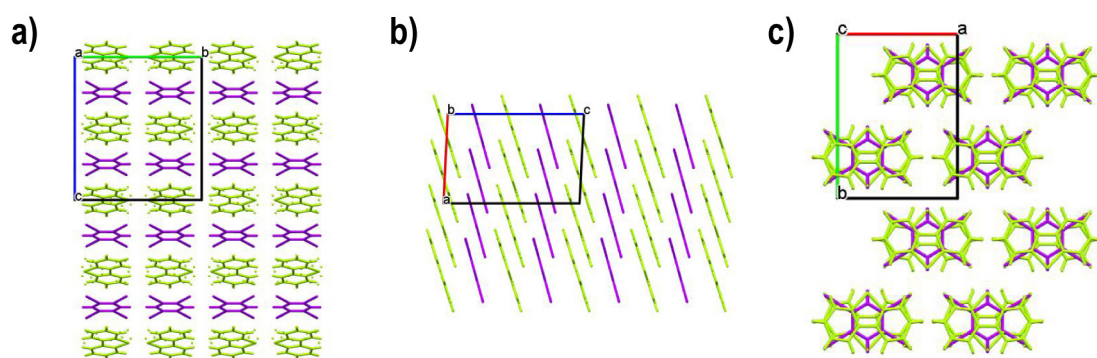


Figure S6. Packing mode of DBS-TCNB-b charge-transfer cocrystal. View along a axis (a), along b axis (b), along c axis (c).

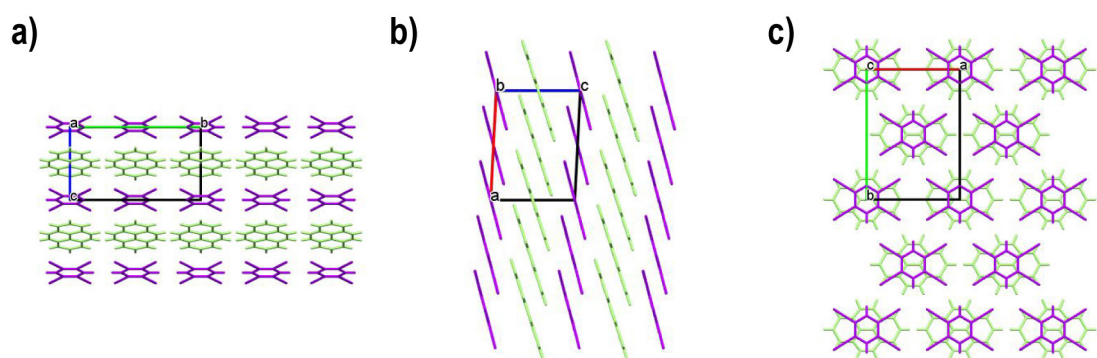


Figure S7. Packing mode of PHT-TCNB-b charge-transfer cocrystal. View along a axis (a), along b axis (b), along c axis (c).

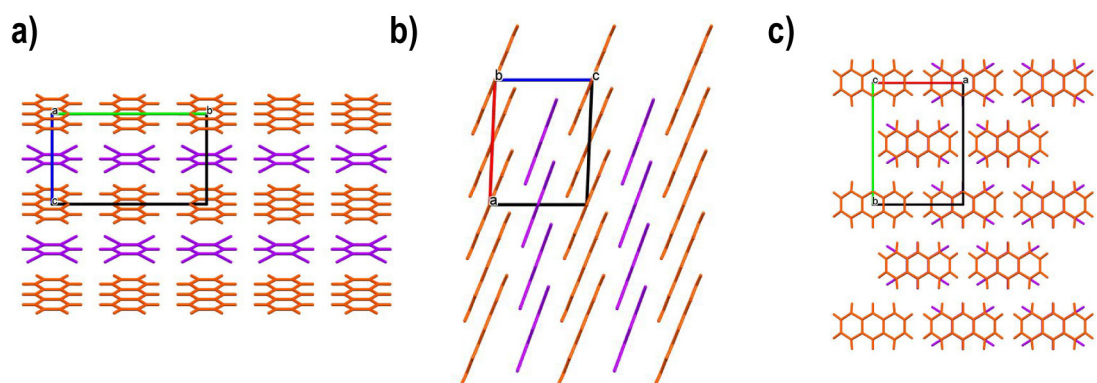


Figure S8. Packing mode of ANT-TCNB-b charge-transfer cocrystal. View along *a* axis (a), along *b* axis (b), along *c* axis (c).

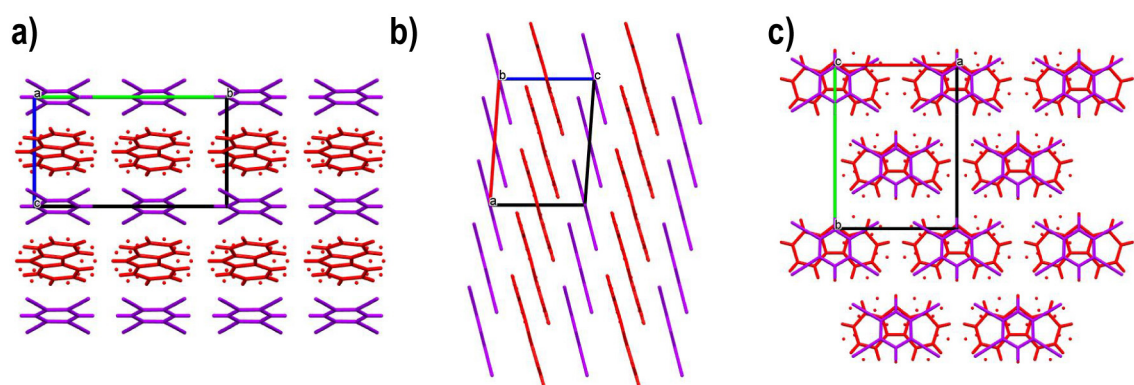


Figure S9. Packing mode of CBZ-TCNB-b charge-transfer cocrystal. View along *a* axis (a), along *b* axis (b), along *c* axis (c).

Packing mode of three herringbone-packing charge-transfer cocrystals

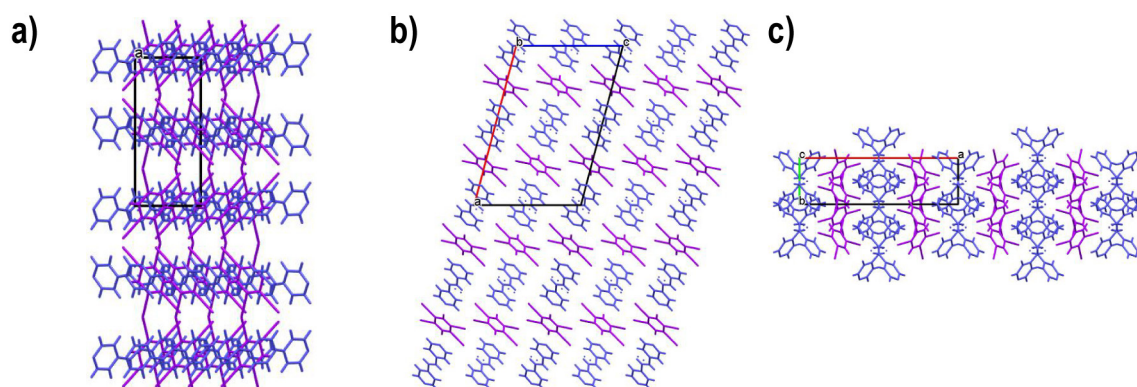


Figure S10. Packing mode of BPE-TCNB-hb charge-transfer cocrystal. View along a axis (a), along b axis (b), along c axis (c).

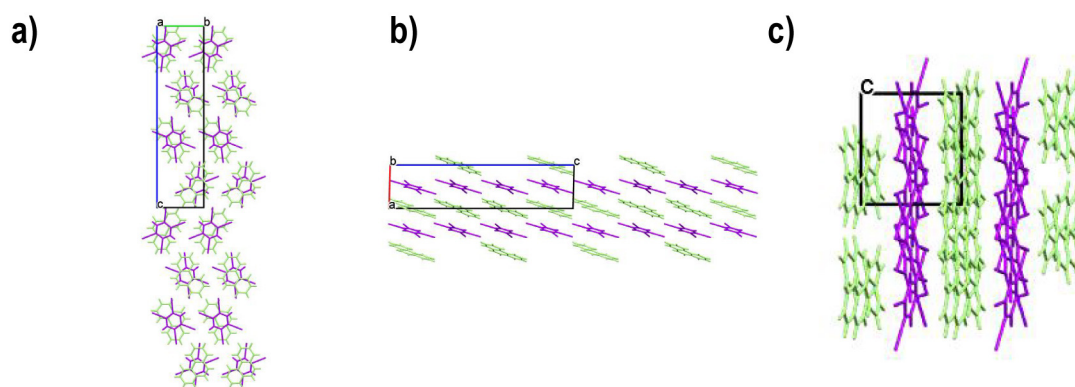


Figure S11. Packing mode of PHT-TCNB-hb charge-transfer cocrystal. View along a axis (a), along b axis (b), along c axis (c).

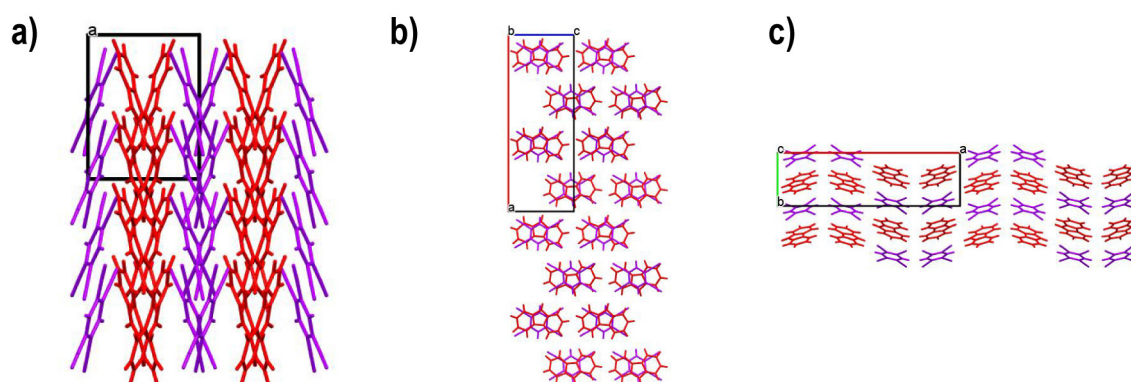


Figure S12. Packing mode of CBZ-TCNB-hb charge-transfer cocrystal. View along a axis (a), along b axis (b), along c axis (c).

X-ray diffraction patterns of single crystals

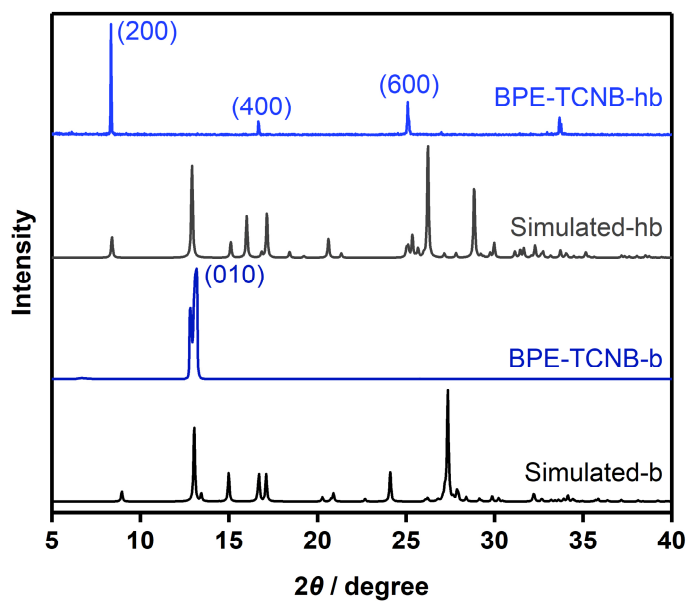


Figure S13. Simulated crystallographic diffraction pattern of BPE-TCNB-b and BPE-TCNB-hb (simulated from available single crystal structure from the Cambridge structural database, CCDC 1405953, CCDC 2017789) and X-ray diffraction pattern of the prepared BPE-TCNB-b and BPE-TCNB-hb single crystal.

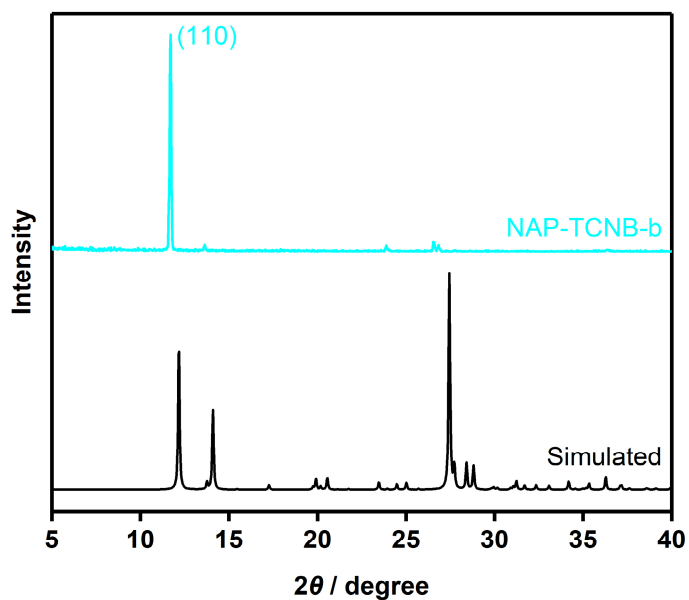


Figure S14. Simulated crystallographic diffraction pattern of NAP-TCNB-b (simulated from available single crystal structure from the Cambridge structural database, CCDC 1216897) and X-ray diffraction pattern of the prepared NAP-TCNB-b single crystal.

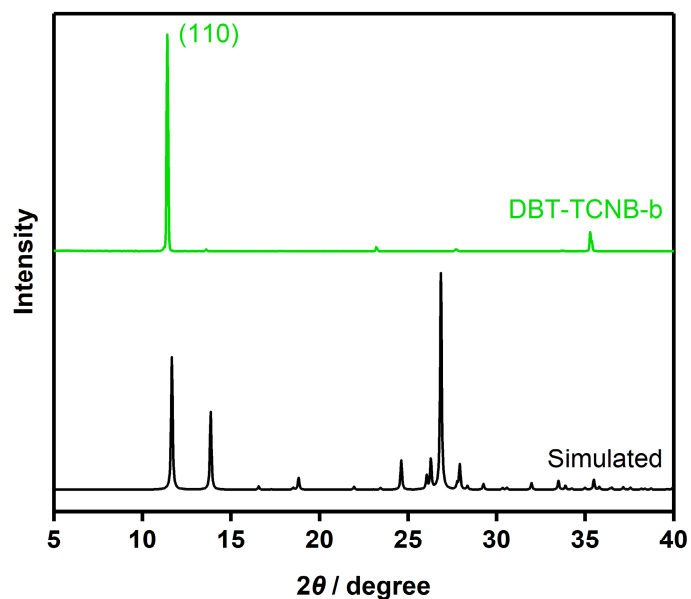


Figure S15. Simulated crystallographic diffraction pattern of DBT-TCNB-b (simulated from available single crystal structure from the Cambridge structural database, CCDC 1481907) and X-ray diffraction pattern of the prepared DBT-TCNB-b single crystal.

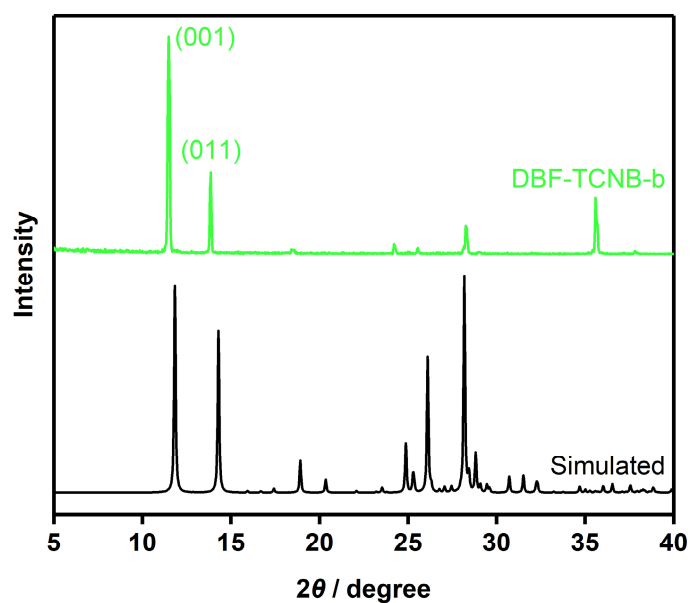


Figure S16. Simulated crystallographic diffraction pattern of DBF-TCNB-b (simulated from available single crystal structure from the Cambridge structural database, CCDC 1967486) and X-ray diffraction pattern of the prepared DBF-TCNB-b single crystal.

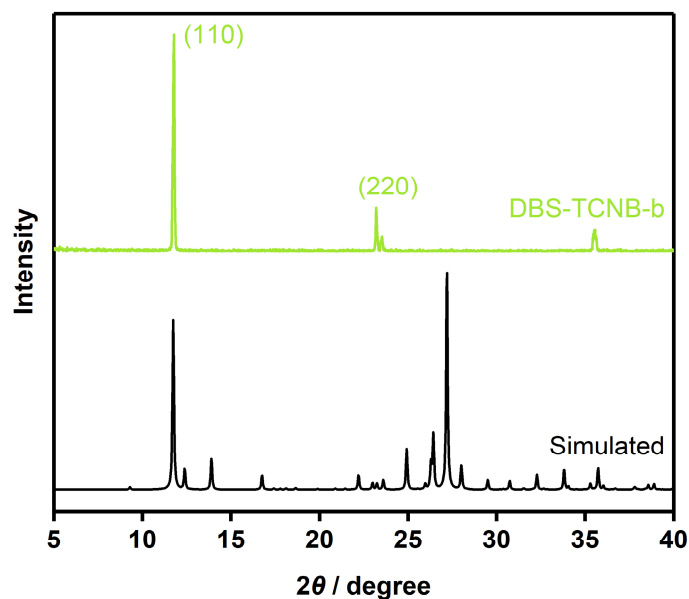


Figure S17. Simulated crystallographic diffraction pattern of DBS-TCNB-b (simulated from available single crystal structure from the Cambridge structural database, CCDC 2056561) and X-ray diffraction pattern of the prepared DBS-TCNB-b single crystal.

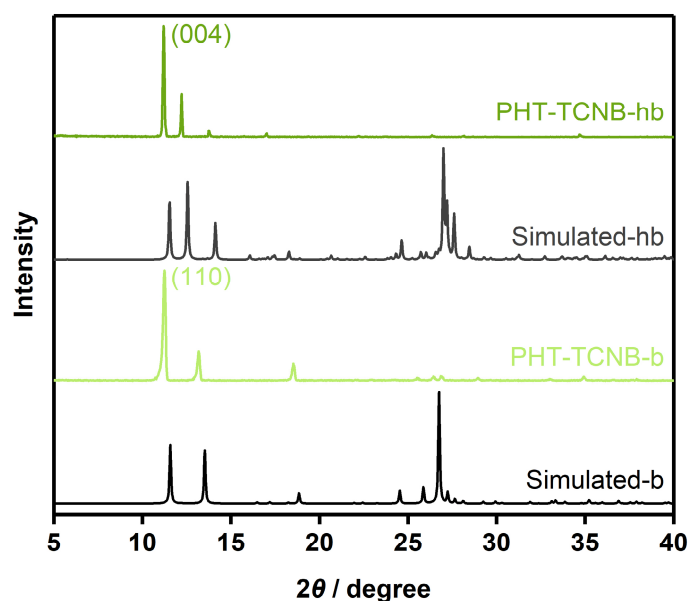


Figure S18. Simulated crystallographic diffraction pattern of PHT-TCNB-b and PHT-TCNB-hb (simulated from available single crystal structure from the Cambridge structural database, CCDC 2013883, CCDC 1967483) and X-ray diffraction pattern of the prepared PHT-TCNB-b and PHT-TCNB-hb single crystal.

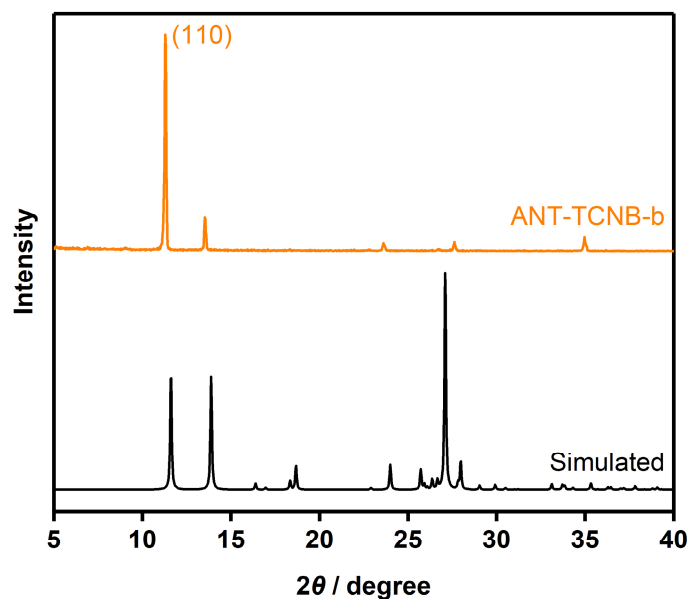


Figure S19. Simulated crystallographic diffraction pattern of ANT-TCNB-b (simulated from available single crystal structure from the Cambridge structural database, CCDC 1103080) and X-ray diffraction pattern of the prepared ANT-TCNB-b single crystal.

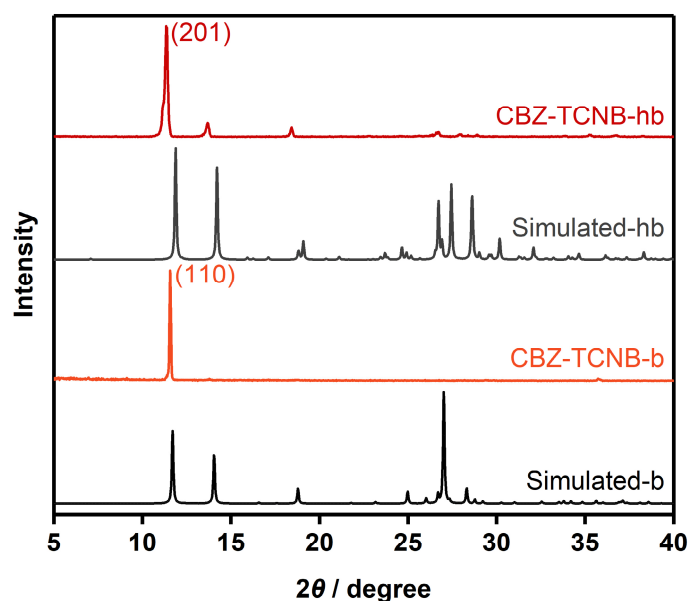


Figure S20. Simulated crystallographic diffraction pattern of CBZ-TCNB-b, CBZ-TCNB-hb (simulated from available single crystal structure from the Cambridge structural database, CCDC 1967476, CCDC 1967490) and X-ray diffraction pattern of the prepared CBZ-TCNB-b, CBZ-TCNB-hb single crystal.

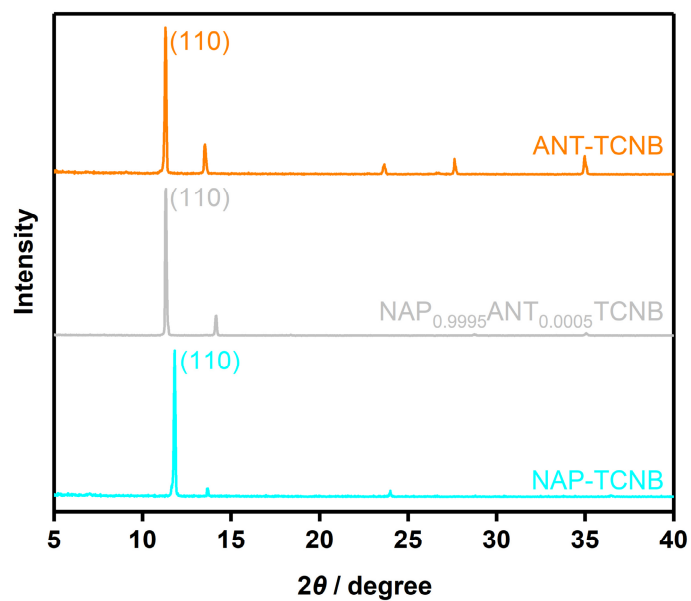


Figure S21. X-ray diffraction pattern of the prepared NAP-TCNB, ANT-TCNB and charge-transfer solid solution $\text{NAP}_{0.9995}\text{ANT}_{0.0005}\text{TCNB}$ single crystal.

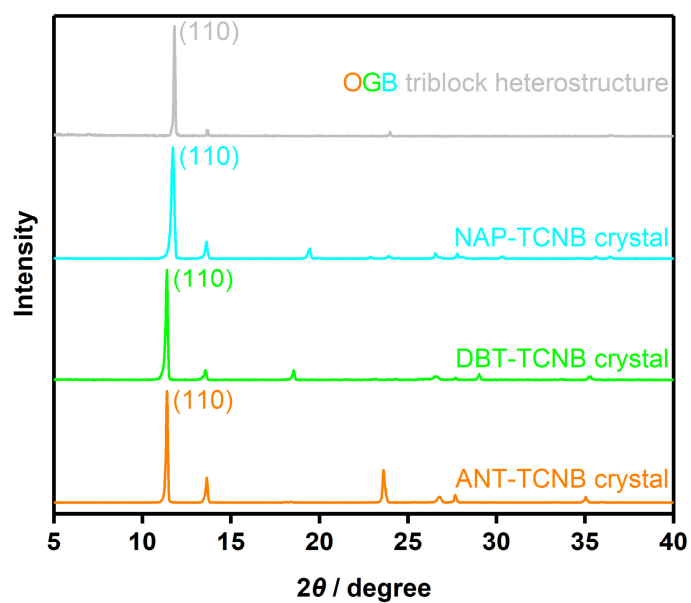


Figure S22. X-ray diffraction pattern of the prepared of OGB triblock heterostructure, ANT-TCNB, DBT-TCNB and NAP-TCNB single crystal.

Photoluminescence Characterizations

Table S2. Photoluminescence properties of a series of organic charge-transfer cocrystals

Crystal	Maximum Absorption Wavenumber/nm	Maximum Emission Wavenumber/nm	Absolute Quantum Yield/%	Lifetime/ns
BPE-TCNB-b	373	415	3.06	11.28
BPE-TCNB-hb	253	426	3.29	12.72
NAP-TCNB-b	406	476	23.05	13.15
DBT-TCNB-b	445	506	59.61	13.51
DBF-TCNB-b	415	520	41.38	103.62
DBS-TCNB-b	433	525	42.00	1205.70
PHT-TCNB-b	440	541	30.08	73.29
PHT-TCNB-hb	438	549	31.96	63.21
ANT-TCNB-b	459	593	23.47	12.35
CBZ-TCNB-b	450	633	4.19	17.85
CBZ-TCNB-hb	438	640	6.49	13.60

Photoluminescence spectrum of TCNB

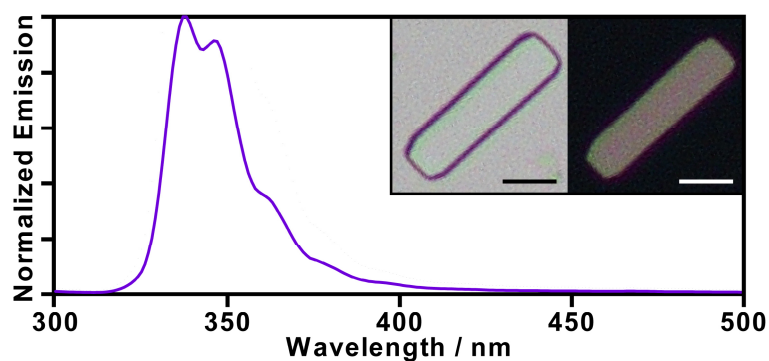


Figure S23. Photoluminescence spectra of TCNB crystals under an excitation wavelength of 285 nm. Inset: optical microphotograph under both bright (standard white light source, left) and dark field (365 nm UV light source, right). Scale bar, 10 μm .

Luminescence lifetime measurement and analysis of eight kinds of brick-packing charge-transfer cocrystals

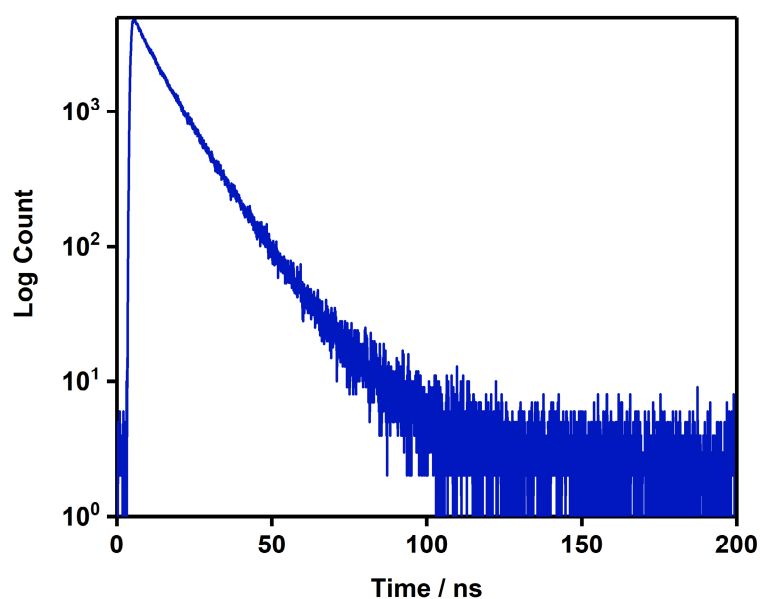


Figure S24. Luminescence lifetime measurement of BPE-TCNB-b cocrystals (at 415 nm, 11.28 ns), calculated from two lifetimes which are 7.67 ns with 42% donation and 13.90 ns with 58% donation) under an excitation wavelength of 373 nm.

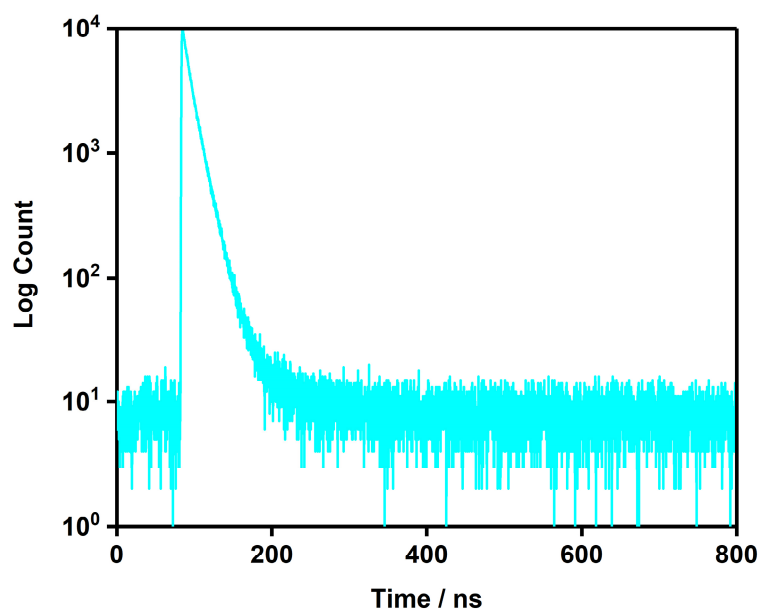


Figure S25. Luminescence lifetime measurement of NAP-TCNB-b cocrystals (at 476 nm, 13.15 ns), calculated from two lifetimes which are 9.94 ns with 65% donation and 19.12 ns with 35% donation) under an excitation wavelength of 373 nm.

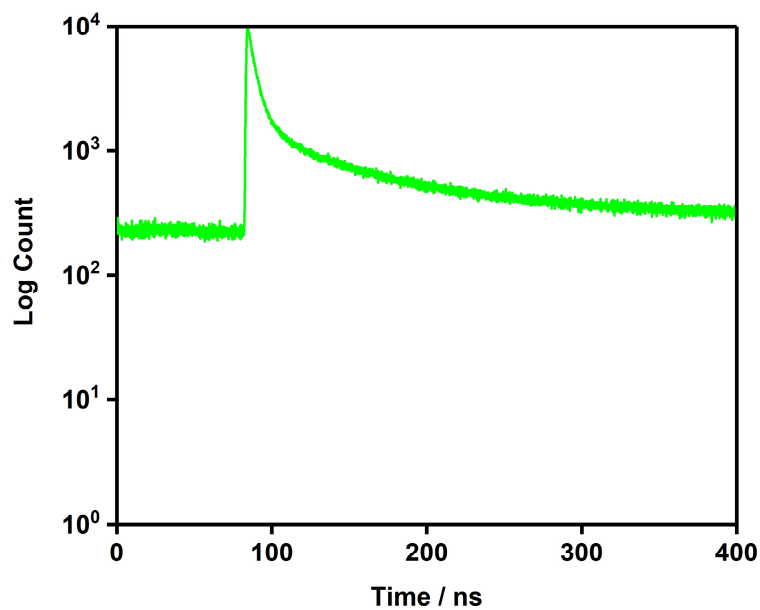


Figure S26. Luminescence lifetime measurement of DBT-TCNB-b cocrystals (at 506 nm, 13.51 ns), calculated from two lifetimes which are 5.97 ns with 90% donation and 81.41 ns with 10% donation) under an excitation wavelength of 373 nm.

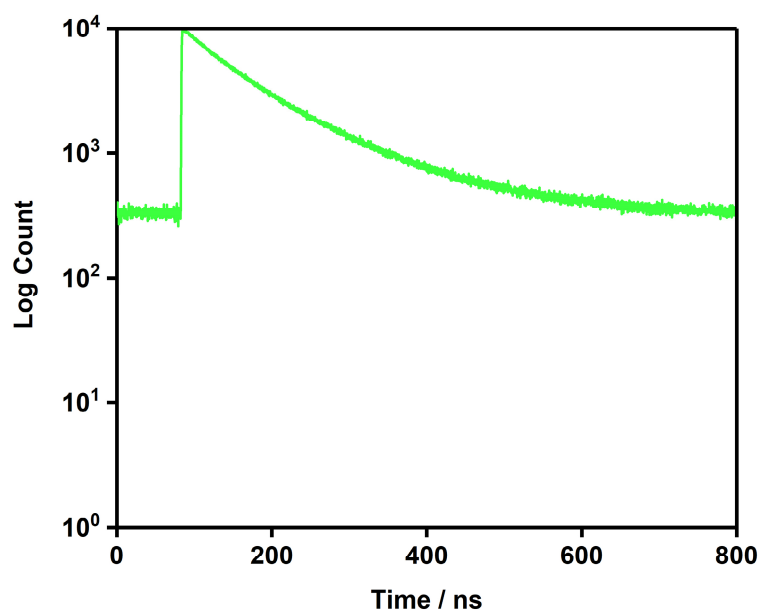


Figure S27. Luminescence lifetime measurement of DBF-TCNB-b cocrystals (at 520 nm, 103.62 ns), calculated from two lifetimes which are 55.59 ns with 41% donation and 137.0 ns with 59% donation) under an excitation wavelength of 373 nm.

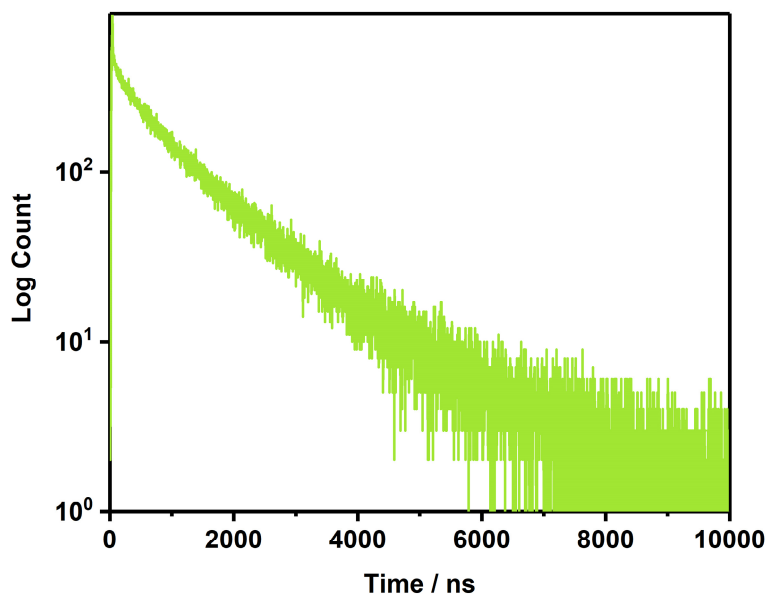


Figure S28. Luminescence lifetime measurement of DBS-TCNB-b cocrystals (at 525 nm, 1205.70 ns), calculated from two lifetimes which are 324.87 ns with 15% donation and 1361.14 ns with 85% donation) under an excitation wavelength of 445 nm.

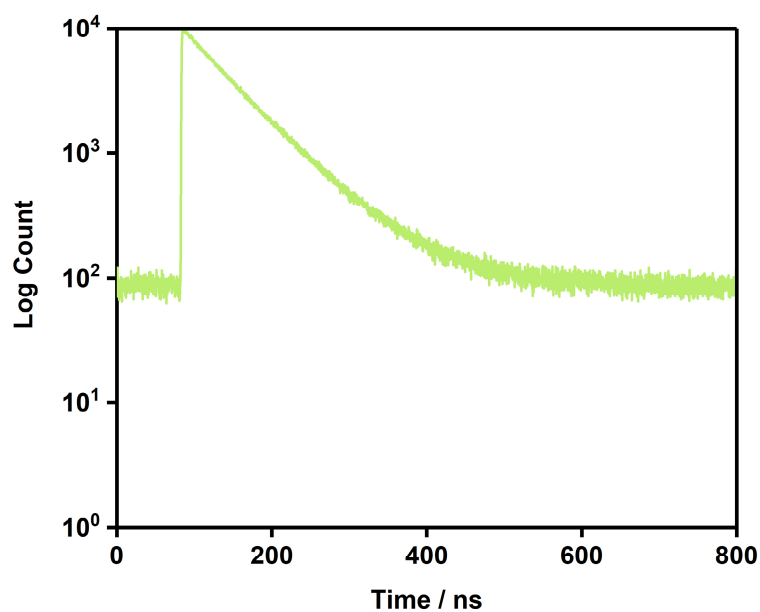


Figure S29. Luminescence lifetime measurement of PHT-TCNB-b cocrystals (at 541 nm, 73.29 ns), calculated from two lifetimes which are 43.55 ns with 14% donation and 78.13 ns with 86% donation) under an excitation wavelength of 445 nm.

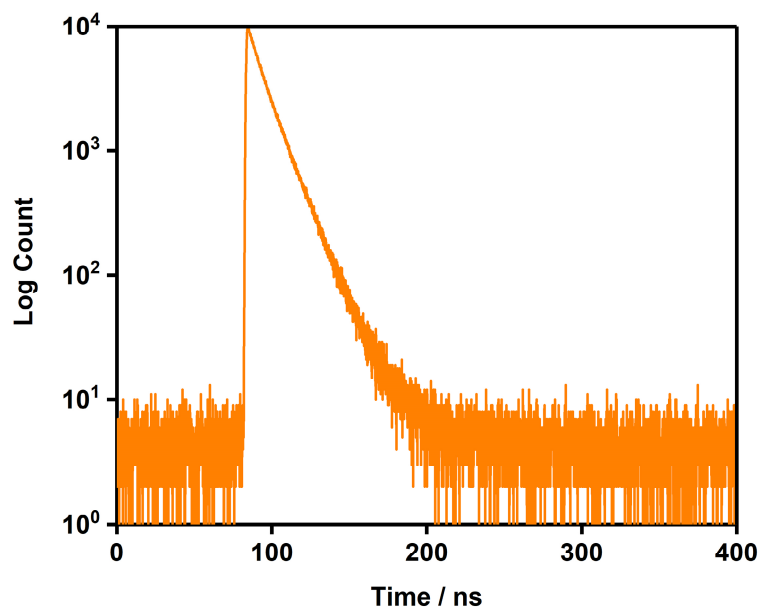


Figure S30. Luminescence lifetime measurement of ANT-TCNB-b cocrystals (at 593 nm, 12.35 ns), calculated from two lifetimes which are 7.04 ns with 37% donation and 15.48 ns with 63% donation) under an excitation wavelength of 445 nm.

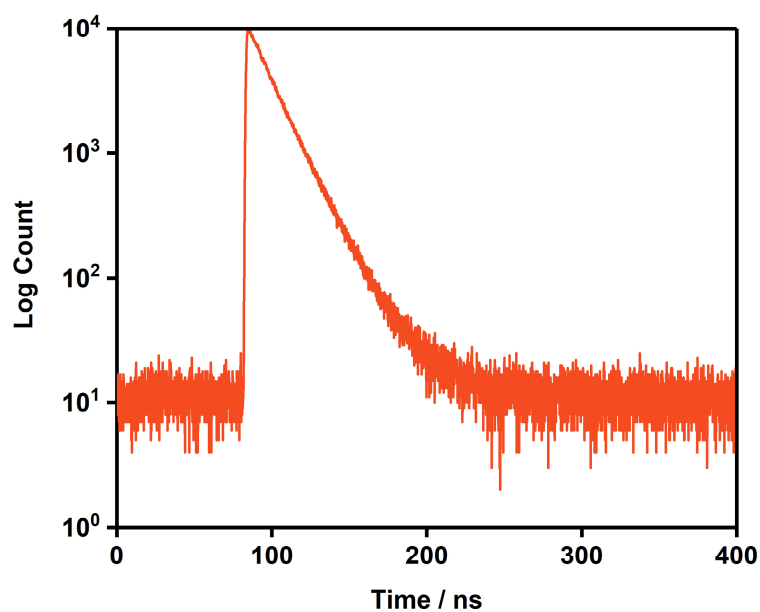


Figure S31. Luminescence lifetime measurement of CBZ-TCNB-b cocrystals (at 633 nm, 17.85 ns), calculated from two lifetimes which are 16.39 ns with 83% donation and 25.00 ns with 17% donation) under an excitation wavelength of 445 nm.

Luminescence lifetime measurement and analysis of three kinds of herringbone-packing charge-transfer cocrystals

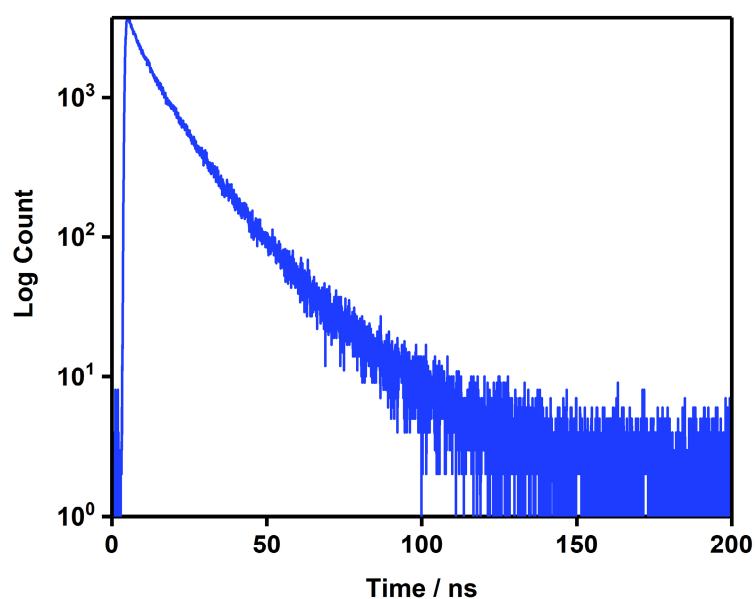


Figure S32. Luminescence lifetime measurement of BPE-TCNB-hb cocrystals (at 425 nm, 12.72 ns), calculated from two lifetimes which are 6.76 ns with 41% donation and 16.87 ns with 59% donation) under an excitation wavelength of 373 nm.

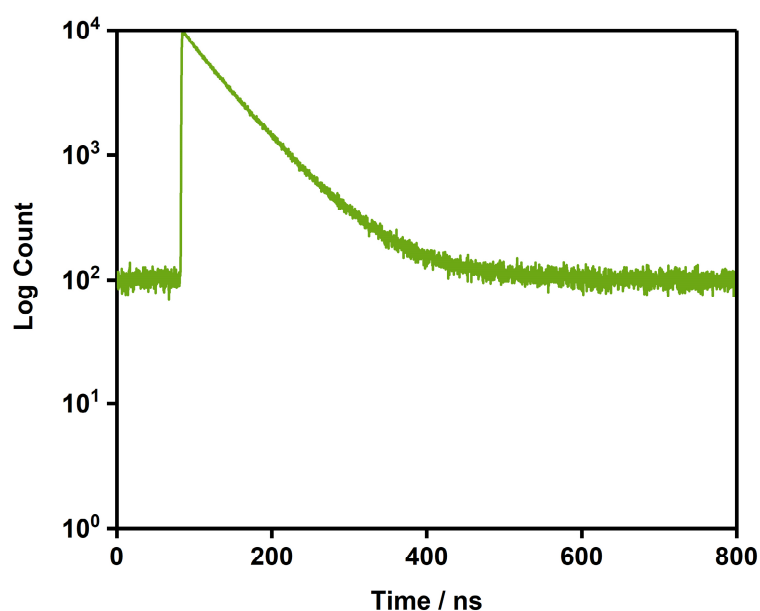


Figure S33. Luminescence lifetime measurement of PHT-TCNB-hb cocrystals (at 549 nm, 63.21 ns), calculated from two lifetimes which are 20.28 ns with 10% donation and 67.98 ns with 90% donation) under an excitation wavelength of 445 nm.

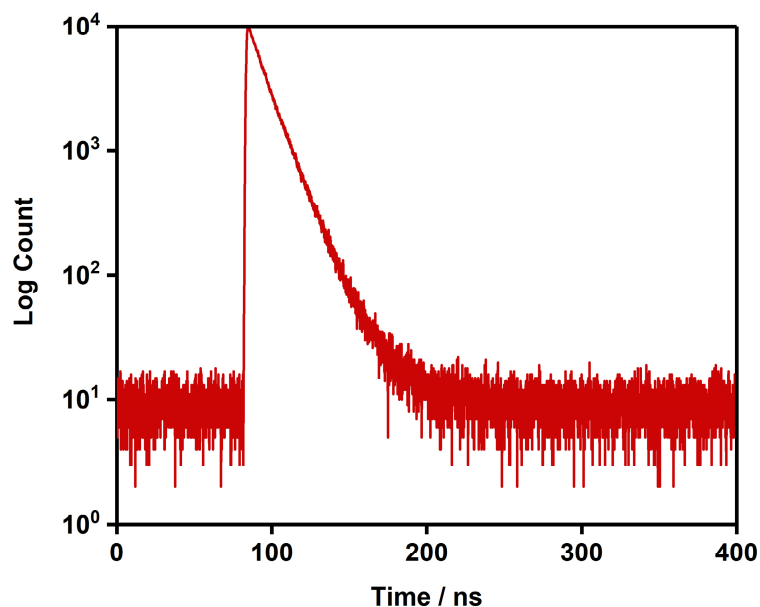


Figure S34. Luminescence lifetime measurement of CBZ-TCNB-hb cocrystals (at 640 nm, 13.60 ns), calculated from two lifetimes which are 11.58 ns with 69% donation and 18.08 ns with 31% donation) under an excitation wavelength of 445 nm.

Luminescence anisotropy measurement of charge-transfer cocrystals

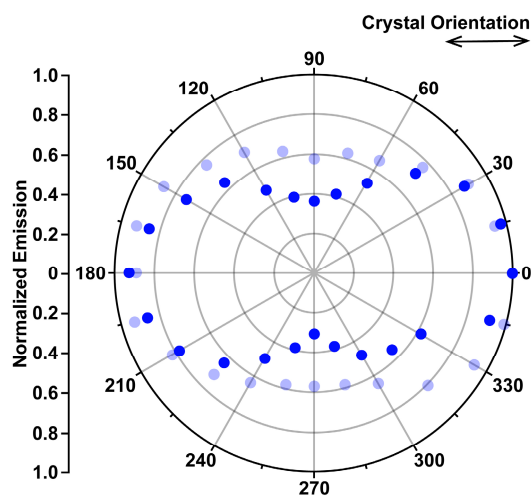


Figure 35. Luminescence spatial polarization profile of BPE-TCNB-b single crystal (deep blue spots) and BPE-TCNB-hb single crystal (light blue spots) under an excitation wavelength of 373 nm.

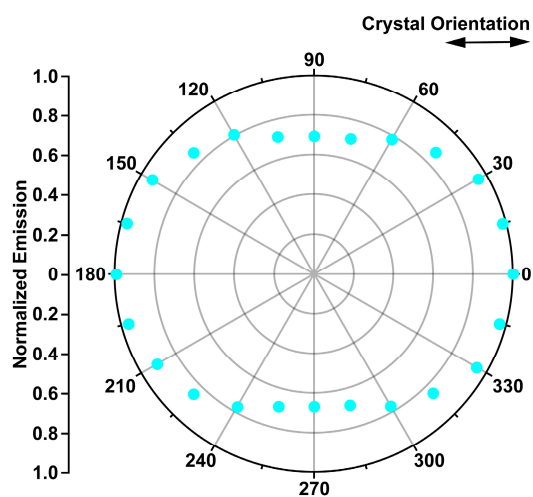


Figure 36. Luminescence spatial polarization profile of NAP-TCNB-b single crystal (cyan spots) under an excitation wavelength of 365 nm.

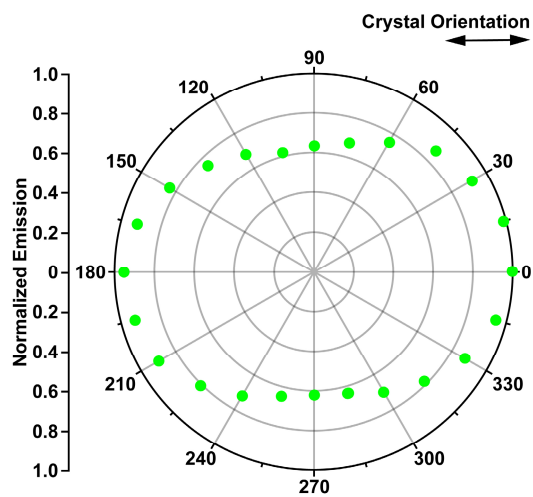


Figure 37. Luminescence spatial polarization profile of DBT-TCNB-b single crystal (green spots) under an excitation wavelength of 365 nm.

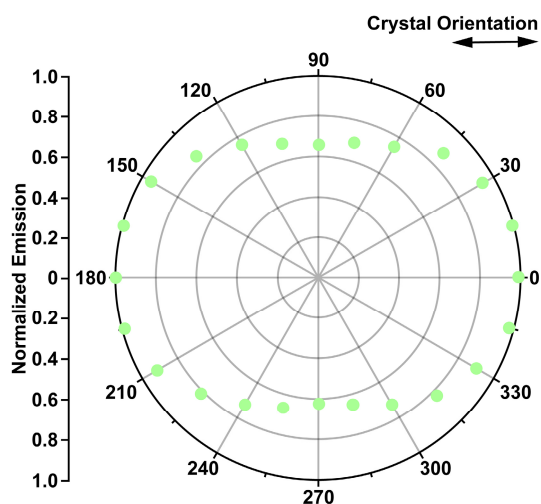


Figure 38. Luminescence spatial polarization profile of DBF-TCNB-b single crystal (light green spots) under an excitation wavelength of 365 nm.

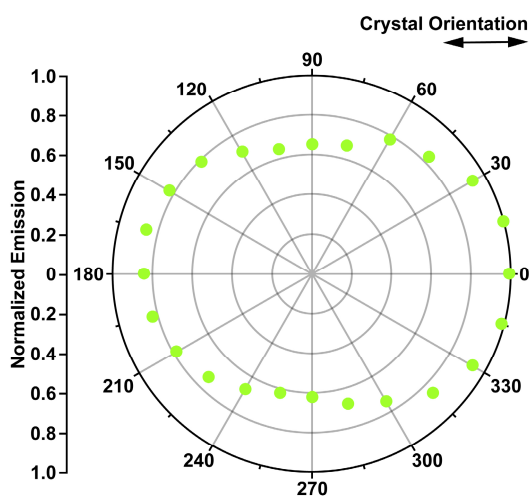


Figure 39. Luminescence spatial polarization profile of DBS-TCNB-b single crystal (yellow green spots) under an excitation wavelength of 365 nm.

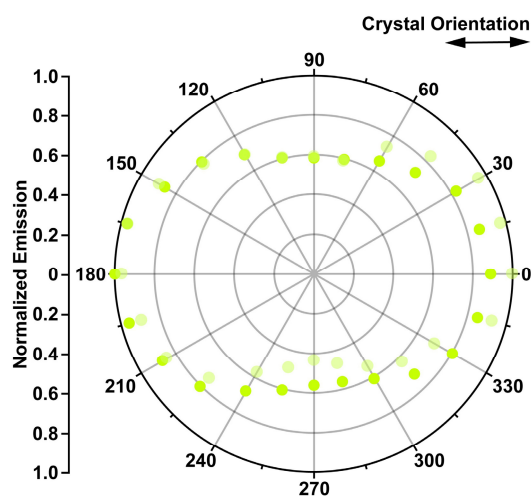


Figure 40. Luminescence spatial polarization profile of PHT-TCNB-b single crystal (deep yellow-green spots) and PHT-TCNB-hb single crystal (light yellow-green spots) under an excitation wavelength of 445 nm.

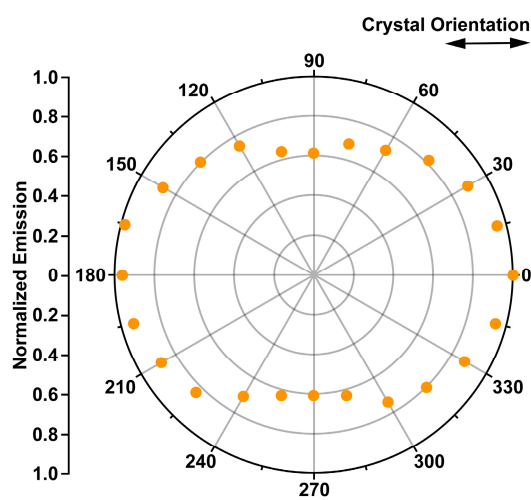


Figure 41. Luminescence spatial polarization profile of ANT-TCNB-b single crystal (orange spots) under an excitation wavelength of 460 nm.

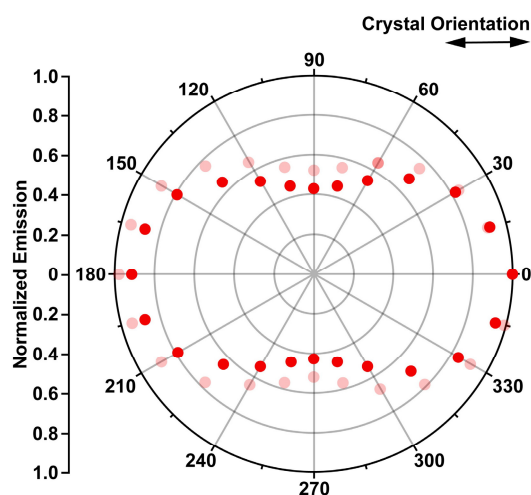


Figure 42. Luminescence spatial polarization profile of CBZ-TCNB-b single crystal (deep red spots) and CBZ-TCNB-hb single crystal (light red spots) under an excitation wavelength of 445 nm.

Photoluminescence properties of charge-transfer complexes in binary solvents (MeCN/H₂O)

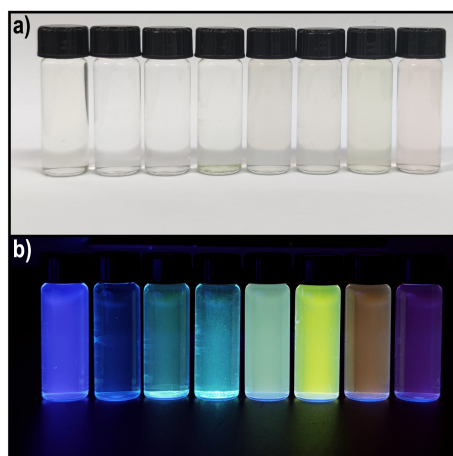


Figure S43. Photographs of eight charge-transfer complexes BPE-TCNB, NAP-TCNB, DBT-TCNB, DBF-TCNB, DBS-TCNB, PHT-TCNB, ANT-TCNB, CBZ-TCNB (from left to right) in binary solvents (MeCN/H₂O=1/40, volume ratio) under daylight lamp (a) and 365 nm UV lamp (b), respectively. Concentration, 0.125 mmol/L.

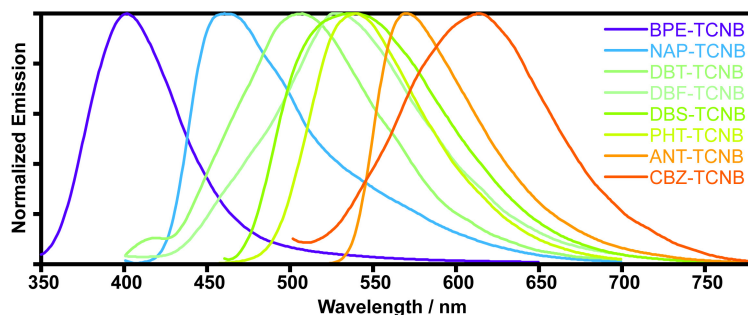


Figure S44. Luminescence spectra of eight kinds of charge-transfer complexes BPE-TCNB, NAP-TCNB, DBT-TCNB, DBF-TCNB, DBS-TCNB, PHT-TCNB, ANT-TCNB, CBZ-TCNB (from left to right) in MeCN/H₂O solution (1/40, volume ratio). Concentration, 0.125 mmol/L.

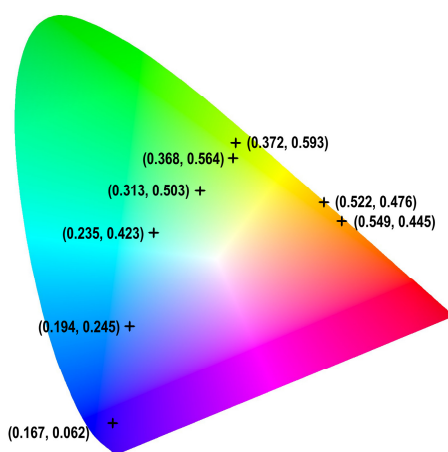


Figure S45. CIE 1931 chromaticity diagram of eight kinds of charge-transfer complexes BPE-TCNB, NAP-TCNB, DBT-TCNB, DBF-TCNB, DBS-TCNB, PHT-TCNB, ANT-TCNB, CBZ-TCNB (from left to right in MeCN/H₂O solution (1/40, volume ratio). Concentration, 0.125 mmol/L. The eight points indicated by crosses signify the color coordinates calculated from the luminescence spectra of different charge-transfer complexes, BPE-TCNB (0.167, 0.062), NAP-TCNB (0.194, 0.245), DBT-TCNB (0.235, 0.423), DBF-TCNB (0.313, 0.503), DBS-TCNB (0.368, 0.564), PHT-TCNB (0.372, 0.593), ANT-TCNB (0.522, 0.476) and CBZ-TCNB (0.549, 0.445), agreed with the direct-recording luminescence colors in Figure S43.

Photoluminescence properties of charge-transfer complexes in binary solvents (DMF/H₂O)

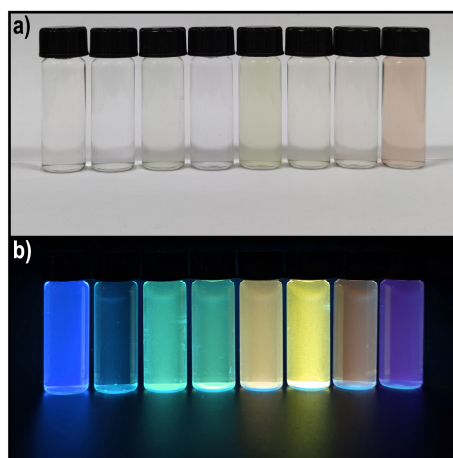


Figure S46. Photographs of eight charge-transfer complexes BPE-TCNB, NAP-TCNB, DBT-TCNB, DBF-TCNB, DBS-TCNB, PHT-TCNB, ANT-TCNB, CBZ-TCNB (from left to right) in binary solvents (DMF/H₂O=1/80, volume ratio) under daylight lamp (a) and 365 nm UV lamp (b), respectively. Concentration, 0.125 mmol/L.

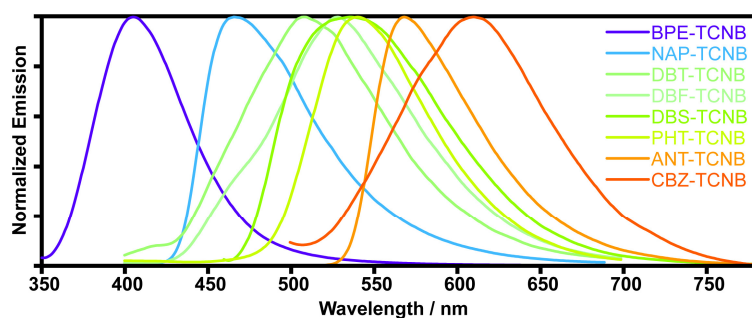


Figure S47. Luminescence spectra of eight kinds of charge-transfer complexes BPE-TCNB, NAP-TCNB, DBT-TCNB, DBF-TCNB, DBS-TCNB, PHT-TCNB, ANT-TCNB, CBZ-TCNB (from left to right) in binary solvents (DMF/H₂O=1/80, volume ratio). Concentration, 0.125 mmol/L.

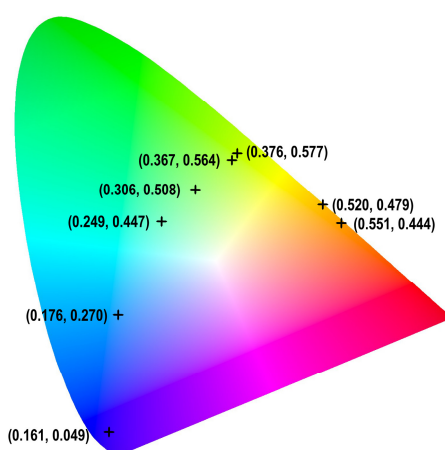


Figure S48. CIE 1931 chromaticity diagram of eight kinds of charge-transfer complexes BPE-TCNB, NAP-TCNB, DBT-TCNB, DBF-TCNB, DBS-TCNB, PHT-TCNB, ANT-TCNB and CBZ-TCNB in binary solvents (DMF/H₂O=1/80, volume ratio). Concentration, 0.125 mmol/L. The eight points indicated by crosses signify the color coordinates calculated from the luminescence spectra of BPE-TCNB (0.161, 0.049), NAP-TCNB (0.176, 0.270), DBT-TCNB (0.249, 0.447), DBF-TCNB (0.306, 0.508), DBS-TCNB (0.367, 0.564), PHT-TCNB (0.376, 0.577), ANT-TCNB (0.520, 0.479), CBZ-TCNB (0.551, 0.444), agreed with the direct-recording luminescence colors in Figure S46.

Density Functional Theory Computations

The calculations of the energy levels were using density functional theory by Gaussian 09 program.^{S1} The molecular structure of eight kinds of donors and acceptor TCNB were optimized and the molecular orbitals were obtained at the B3LYP/6-31G (d) level.

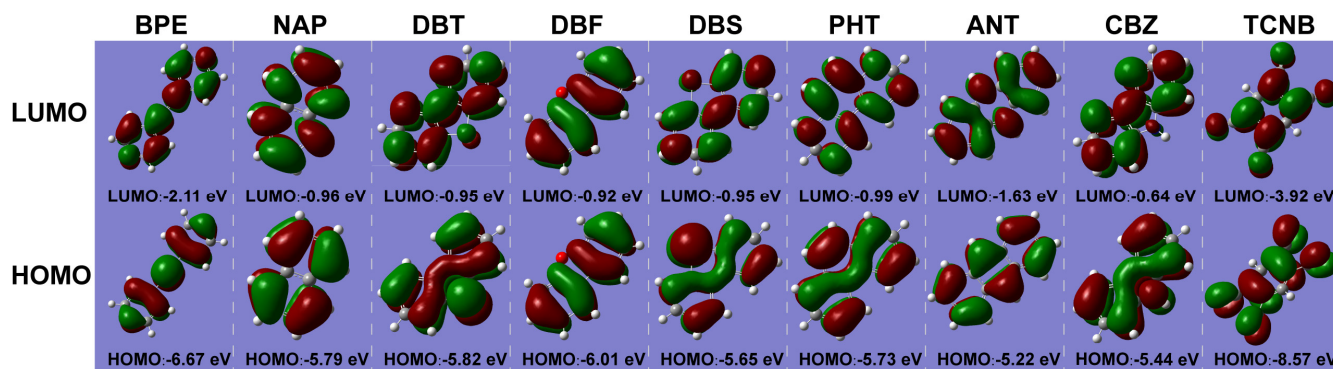


Figure S49. Highest occupied molecular orbital (HOMO) and lowest unoccupied molecular orbital (LUMO) of eight kinds of donors BPE, NAP, DBT, DBF, DBS, PHT, ANT, CBZ and acceptor TCNB.

Jabloński Diagram of the Charge-Transfer Complex

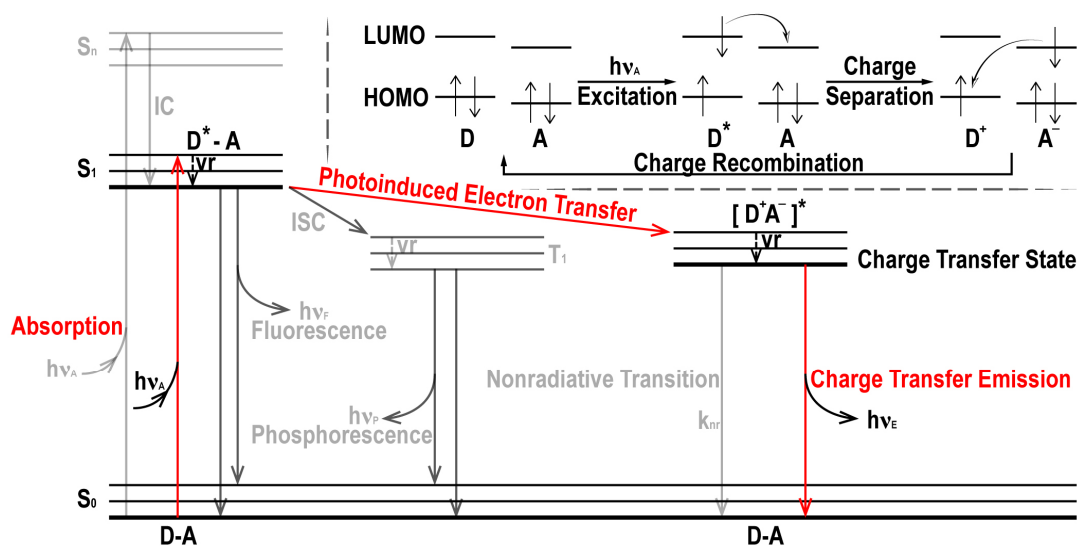


Figure S50. Jablonski diagram of the charge-transfer complex.

The electron donor and electron acceptor self-assemble into a charge-transfer complex D-A (ground state, the lowest energy) through charge-transfer interaction. With the absorption of light ($h\nu_A$), the charge-transfer complex was excited to higher vibrational level S_1 , or S_n , in which an electron transitions from HOMO of donor to its LUMO, as $[D^*A]$. S_n experienced after internal conversion (IC) to the lowest vibrational level of S_1 , or through vibrational relaxation (vr) to the lowest vibrational level of S_1 . The excited donor transfers an electron from its LUMO to the LUMO of acceptor, forming the charge-transfer exciplex $[D^+A^-]^*$ accompanied by the release of energy. This exciplex in charge-transfer state may emit a photon and return to the ground state or be quenched or nonradiative decay. Because the vibration or rotation of donors or acceptors molecules is limited in crystal, the nonradiation transition of exciplex is inhibited to the utmost, which leads to charge-transfer emission.

Therefore, the luminescence of charge-transfer complex is dictated to the process of the charge-recombination. The energy difference in this process is not equal to the bandgap between HOMO of donor and LUMO of acceptor but associated with its energy difference between its charge-transfer state and ground state.

The Growth Process of ABA/AB-Type Heterostructures

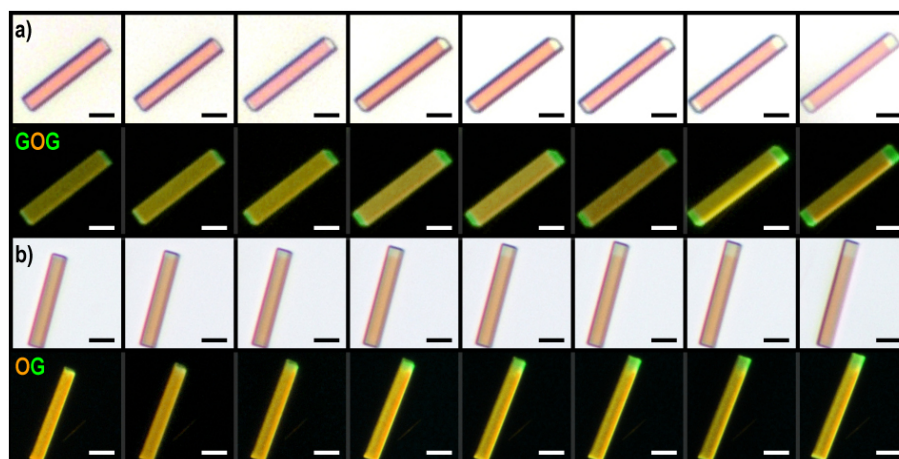


Figure S51. Microscopic observation of the growth process of ABA/AB-type heterostructures. (a) Microphotographs of the growth process GOG triblock heterostructures. (b) Microphotographs of the growth process OG diblock heterostructures. Observed under both bright field (standard white light source) and dark field (365 nm UV light source). Scale bar, 10 μm .

The Conceptual Optical Logic Gate Based on the ABC-Type Heterostructures

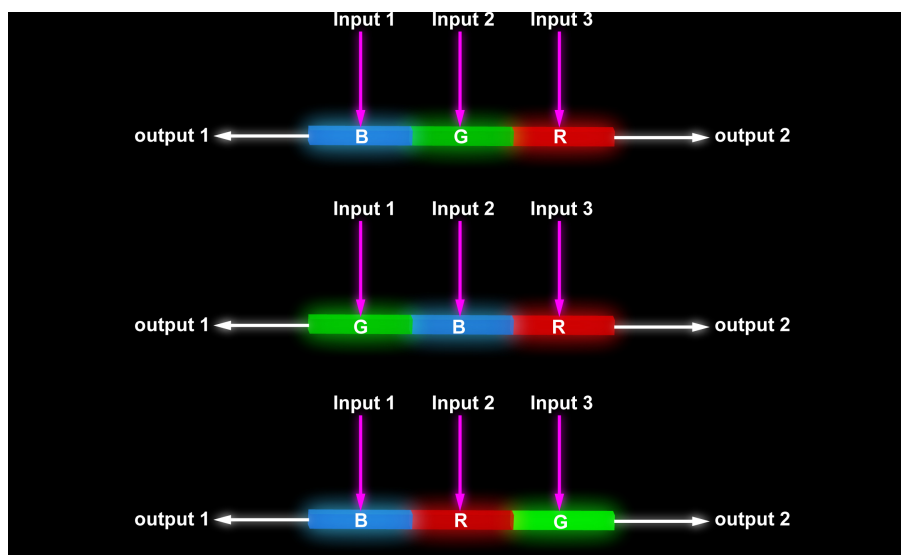


Figure S52. Schematic diagram of ABC-type triblock heterostructures as the optical logic gate.

Table S3. The conceptual truth table of optical logic gate of BGR heterostructure

Input 1	Input 2	Input 3	Output 1			Output 2		
			470 nm	510 nm	630 nm	470 nm	510 nm	630 nm
			(B)	(G)	(R)	(B)	(G)	(R)
1	0	0	1	0	0	0	0	1
0	1	0	1	1	0	0	0	1
0	0	1	1	1	1	0	0	1

Table S4. The conceptual truth table of optical logic gate of GBR heterostructure

Input 1	Input 2	Input 3	Output 1			Output 2		
			470 nm	510 nm	630 nm	470 nm	510 nm	630 nm
			(B)	(G)	(R)	(B)	(G)	(R)
1	0	0	0	1	0	0	0	1
0	1	0	0	1	0	0	0	1
0	0	1	0	1	1	0	0	1

Table S5. The conceptual truth table of optical logic gate of BRG heterostructure

Input 1	Input 2	Input 3	Output 1			Output 2		
			470 nm	510 nm	590 nm	470 nm	510 nm	590 nm
			(B)	(G)	(R)	(B)	(G)	(R)
1	0	0	1	0	0	0	1	1
0	1	0	1	0	1	0	1	1
0	0	1	1	0	1	0	1	0

Reference

(1) Gaussian 09, Revision D.01, M. J. Frisch, G. W. Trucks, H. B. Schlegel, G. E. Scuseria, M. A. Robb, J. R. Cheeseman, G. Scalmani, V. Barone, B. Mennucci, G. A. Petersson, H. Nakatsuji, M. Caricato, X. Li, H. P. Hratchian, A. F. Izmaylov, J. Bloino, G. Zheng, J. L. Sonnenberg, M. Hada, M. Ehara, K. Toyota, R. Fukuda, J. Hasegawa, M. Ishida, T. Nakajima, Y. Honda, O. Kitao, H. Nakai, T. Vreven, J. A. Montgomery, Jr., J. E. Peralta, F. Ogliaro, M. Bearpark, J. J. Heyd, E. Brothers, K. N. Kudin, V. N. Staroverov, T. Keith, R. Kobayashi, J. Normand, K. Raghavachari, A. Rendell, J. C. Burant, S. S. Iyengar, J. Tomasi, M. Cossi, N. Rega, J. M. Millam, M. Klene, J. E. Knox, J. B. Cross, V. Bakken, C. Adamo, J. Jaramillo, R. Gomperts, R. E. Stratmann, O. Yazyev, A. J. Austin, R. Cammi, C. Pomelli, J. W. Ochterski, R. L. Martin, K. Morokuma, V. G. Zakrzewski, G. A. Voth, P. Salvador, J. J. Dannenberg, S. Dapprich, A. D. Daniels, O. Farkas, J. B. Foresman, J. V. Ortiz, J. Cioslowski, and D. J. Fox, *Gaussian, Inc.*, Wallingford CT, **2013**.

Additional Issues

Additional issues are some points not mentioned in the manuscript while discussed with the reviewers.

1. Issue on the Jabłoński diagram and photoinduced electron transfer process

The Jabłoński diagram, named after the Polish physicist Aleksander Jabłoński (1898-1980), is a diagram that illustrates the electronic states of a molecule and the transitions between them. It is a powerful tool for visualizing the possible transitions that can occur after a molecule has been photoexcited.

In many previous reports (*J. Mater. Chem. C* **2020**, 8, 2669-2675, for example), the bandgap of charge-transfer cocrystal is often approximated as the energy difference between the highest occupied molecular orbital (HOMO) of the donor and the lowest unoccupied molecular orbital (LUMO) of the acceptor. In these works, researchers usually reported the optical properties of two or three charge-transfer cocrystals which show great differences in luminescent colors between each other. To some extent, such approximation could explain their experimental findings. Naturally, the traditional cognition, that the smaller energy difference between the HOMO of the donor and the LUMO of the acceptor is, the longer luminescence wavelength of their charge-transfer cocrystals will be, has been widely accepted. However, in our work, a series of eight cocrystals with the same acceptor and eight different donors were constructed, providing rich comparative data. This series of results led us to observe some irrationalities of the traditional views.

We gave the explanation through a Jabłoński diagram (Figure S50) in the Supporting Information. Additionally, three schemes were added to further explain this issue. After the electron donor and the electron acceptor self-assemble into a charge transfer complex, the ground state electrons of the donor will be transferred to the antibonding orbital of the acceptor under light irradiation, as shown in Figure S53. This process could be described in the Jabłoński diagram (Figure S54). With the absorption of light ($h\nu_A$), the charge-transfer complex was excited to higher vibrational level S_n , and then relax to the lowest vibrational level of S_1 . Meanwhile, the ground state electrons of the donor will be transferred to the antibonding orbital of the acceptor as mentioned above, which is the photoinduced electron transfer process. The light was emitted in the process of the electron falling back to the ground state.

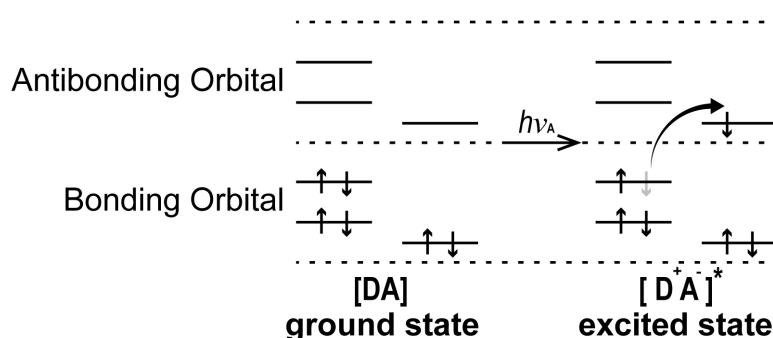


Figure S53. Schematic representation of photoinduced charge transfer transition.

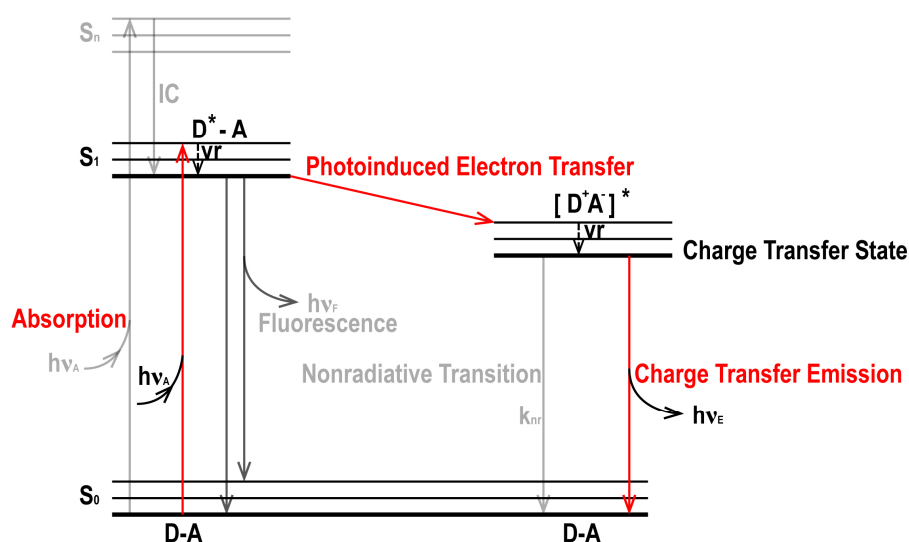


Figure S54. Jablonski diagram of the charge-transfer complex for the illustration of the photoinduced electron transfer process.

Incidentally, in some cases, although the charge-transfer complex cannot be formed in the ground state, it may be formed in the excited state under light irradiation because of the photoinduced electron transfer process (Figure S55).

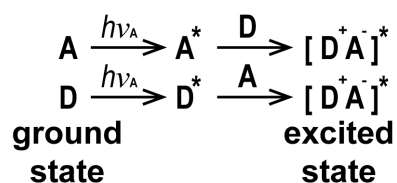


Figure S55. Schematic representation of photoinduced charge transfer process when the donor and the acceptor cannot form charge-transfer complex in the ground state.

2. Detailed method for preparation of the white light-emitting charge-transfer solid solution

Charge-transfer complexes in MeCN/H₂O solution: Take BPE-TCNB for example, BPE (9.3 mg, 0.05 mmol) and TCNB (9.2 mg, 0.05 mmol) were added into 10 mL MeCN solution, dissolved well through ultrasound. And then 0.1 mL prepared MeCN solution of BPE and TCNB were taken out and added into a 5 mL glass bottle. We dilute it with 4 mL pure water to obtain a 0.0125 mmol/L charge-transfer complexes in solution. The preparation methods of the other charge-transfer complexes are the same as above.

3. Issue on the luminescence of different polymorphs

In different crystal structures, the molecular configuration and/or packing are different, resulting in different electron cloud distributions of π -conjugate molecules, thus affecting the optical properties, reflected in luminescence color, intensity and lifetime. Usually, polymorphs display distinct optical properties. Because the optical properties of most luminescent crystals are caused by the orderly arrangement of molecules in the crystal.

What we want to highlight here is that the origin of the luminescence of charge-transfer cocrystals is the charge transfer between the donor and acceptor, rather than the further packing of charge-transfer pairs in crystals. Therefore, polymorphs of charge-transfer cocrystals show a small difference in luminescence, which makes the charge-transfer cocrystal a suitable platform to realize a fine-tuning of the luminescence.

4. Measurement of the photoluminescence anisotropy

The schematic representation of the experimental setup was shown in Figure S-1.

The photographs of this setup were shown in Figure S56.

The polarizer used in this experiment is U-AN360P (OLYMPUS, Japan).

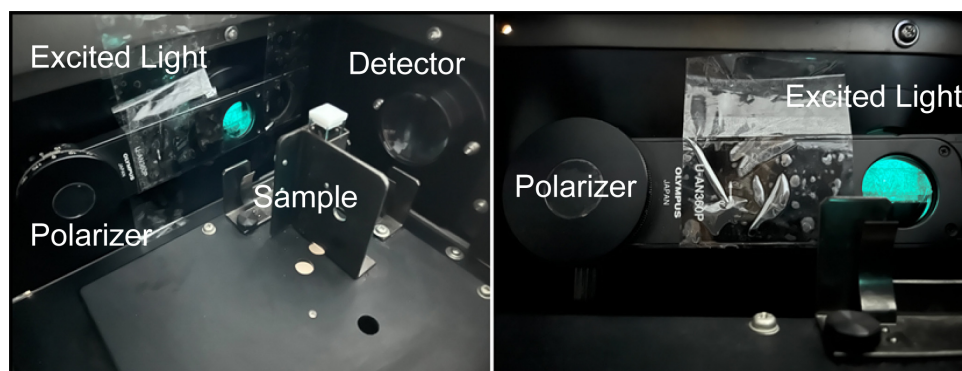


Figure S56. Photographs of the experimental setup for photoluminescence anisotropy characterization.

5. The exact question: The luminescence lifetime of 1.21 microsec for DBS-TCNB-b crystals is remarkable. Please state the reason for this. For example, it could be phosphorescence emission or thermally activated delayed fluorescence.....

We also noticed this unusual numerical value and expressed it in the manuscript, but did not further explain the luminescence mechanism behind this phenomenon.

There is a 1205.70 ns luminescence lifetime of DBS-TCNB-b cocrystal, calculated from two lifetimes which are 324.87 ns with 15% donation and 1361.14 ns with 85% donation (Figure S28).

In order to better answer your question, we measured the micro-second scale photoluminescence lifetime of DBS-TCNB-b using a microsecond flash-lamp at room temperature. The micro-second scale photoluminescence lifetime is calculated as 4.64 μ s (Figure S57), could be regarded as phosphorescence. Considering the fact that the phosphorescence will be enhanced at low temperature due to the limitation of the non-radiative transition pathway, we further measured the micro-second scale photoluminescence lifetime of DBS-TCNB-b at 77 K in vacuum condition. As we expected, the lifetime is 27.19 μ s (Figure S57), indicating that DBS-TCNB-b cocrystal has phosphorescent emission behavior.

We also examined whether the thermally activated delayed fluorescence exists. Unfortunately, we did not get a positive result.

To sum up, we conclude the special long lifetime is caused by phosphorescent emission.

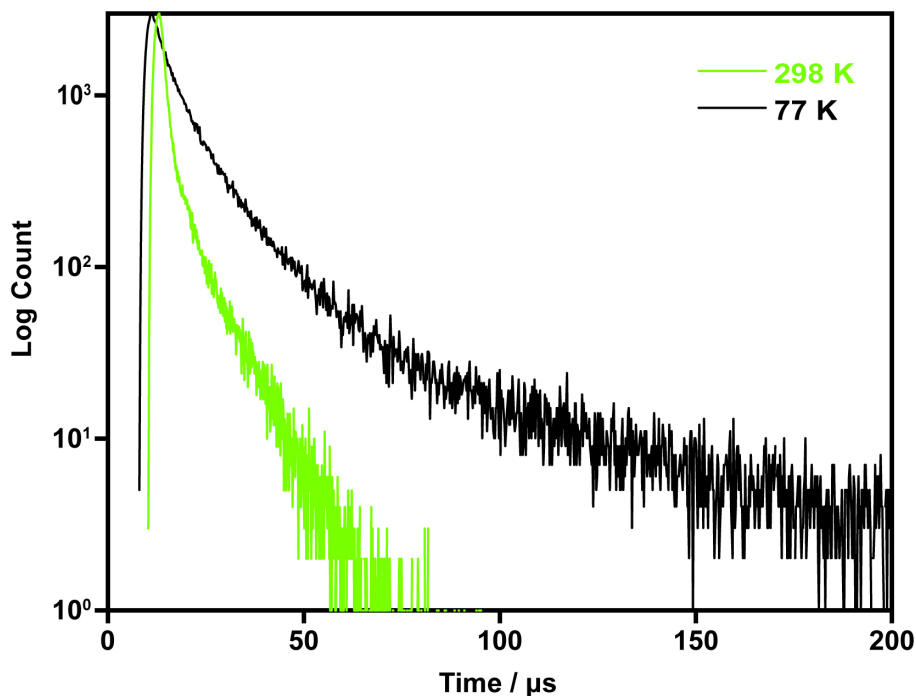


Figure S57. Micro-second scale luminescence lifetime measurement of DBS-TCNB-b cocrystals at 298 K (at 525 nm, 4644.27 ns, calculated from two lifetimes which are 1395.01 ns with 54% donation and 8429.64 ns with 46% donation) and 77 K (at 525 nm, 27.19 μ s, calculated from three lifetimes which are 5.36 μ s with 17% donation and 17.09 μ s with 59% donation and 67.74 μ s with 24% donation) under an excitation wavelength of 433 nm.

6. The exact question: The luminescence lifetime of DBF-TCNB-b crystals is also 103 ns, which is too long for conventional fluorescent material. Please clarify the reason for this by conducting additional experiments.

We measured the micro-second scale photoluminescence lifetime of DBF-TCNB-b using a microsecond flash-lamp at 298 K, and 77 K in vacuum condition. The lifetime at 298 K and 77 K are 16.05 μ s and 4.44 μ s (Figure S58), respectively.

According to the increase in the lifetime of DBF-TCNB-b cocrystal at higher temperature, we infer that the long lifetime may belong to thermally activated delayed fluorescence. More rigorous conclusions need to be verified by in-depth experiments and theoretical calculations, which will proceed in future research.

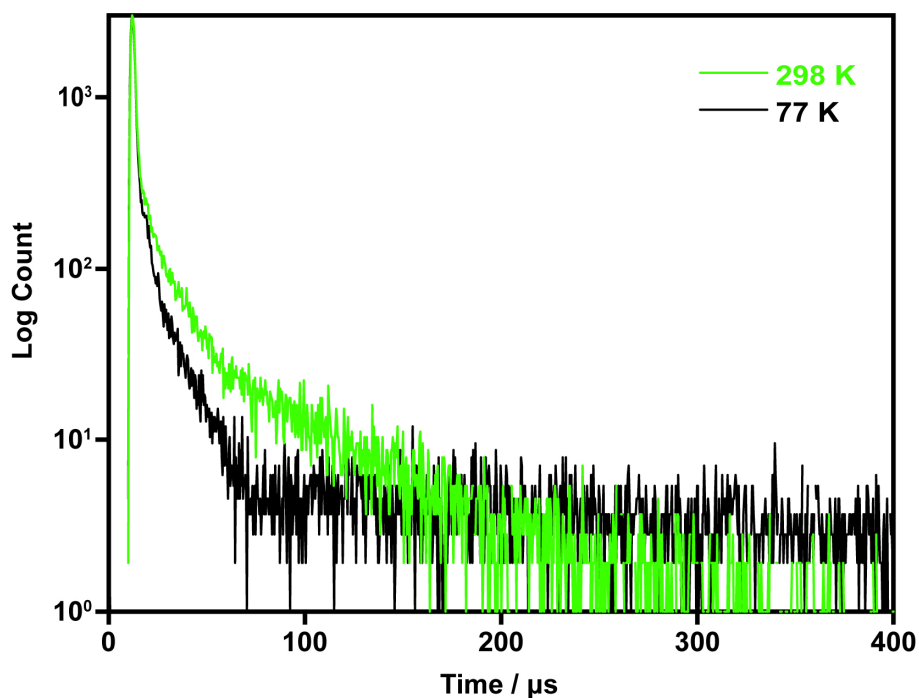


Figure S58. Micro-second scale luminescence lifetime measurement of DBF-TCNB-b cocrystals at 298 K (at 520 nm, 16.05 μ s, calculated from three lifetimes which are 1.11 μ s with 47% donation and 10.67 μ s with 31% donation and 56.57 μ s with 22% donation) and 77 K (at 520 nm, 4.44 μ s, calculated from two lifetimes which are 1.13 μ s with 66% donation and 10.93 μ s with 34% donation) under an excitation wavelength of 415 nm.

7. The exact question: Please evaluate in detail the quantum yield and luminescence lifetime of white luminescent crystals and phase-separated crystals, and summarize the results in supporting information.

We additionally tested the absolute quantum yield and luminescence lifetime of the white light-emitting charge-transfer solid solution and cocrystal heterostructure using a FLS 1000 (Edinburgh Instruments) configured with an integrated sphere.

The absolute quantum yield of white light-emitting charge-transfer solid solution is 19.29%. The luminescence lifetimes are shown in Figure S59, calculated as 13.20 ns at 476 nm and 51.15 ns at 593 nm.

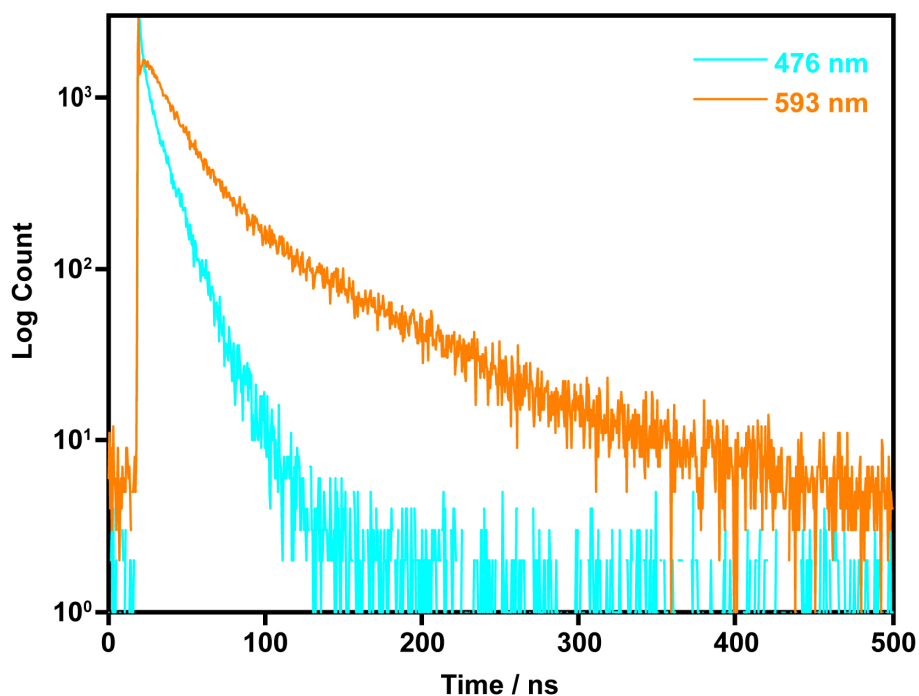


Figure S59. Luminescence lifetime measurement of white light-emitting charge-transfer solid solution (at 476 nm, 13.20 ns, calculated from two lifetimes which are 2.79 ns with 19% donation and 15.68 ns with 81% donation; at 593 nm, 51.15 ns, calculated from two lifetimes which are 22.95 ns with 59% donation and 91.22 ns with 41% donation) under an excitation wavelength of 375 nm.

However, for the heterostructures, the fluorescence measurement is not one easy task. We can not prepare a large number of heterostructures at one time, and not all the prepared crystals are heterostructures. Therefore, we can only artificially select and collect satisfactory samples for testing, which is a time-consuming work. We selected a representative sample, OGB triblock heterostructure, for the quantum yield and luminescence lifetime measurement.

The luminescence lifetime of OGB triblock heterostructure (orange light-emitting ANT-TCNB-b, green light-emitting DBT-TCNB-b, and blue light-emitting NAP-TCNB-b) is shown in Figure S60, calculated as 266.41 ns at 476 nm, 651.56 ns at 506 nm and 456.54 ns at 593 nm. Unexpectedly, the luminescence lifetimes of the blocks in the heterostructure increase compared to each block itself. A further explanation will need in-depth experiments, which will proceed in our future research.

The absolute quantum yield of the OGB triblock heterostructure is 20.76%.

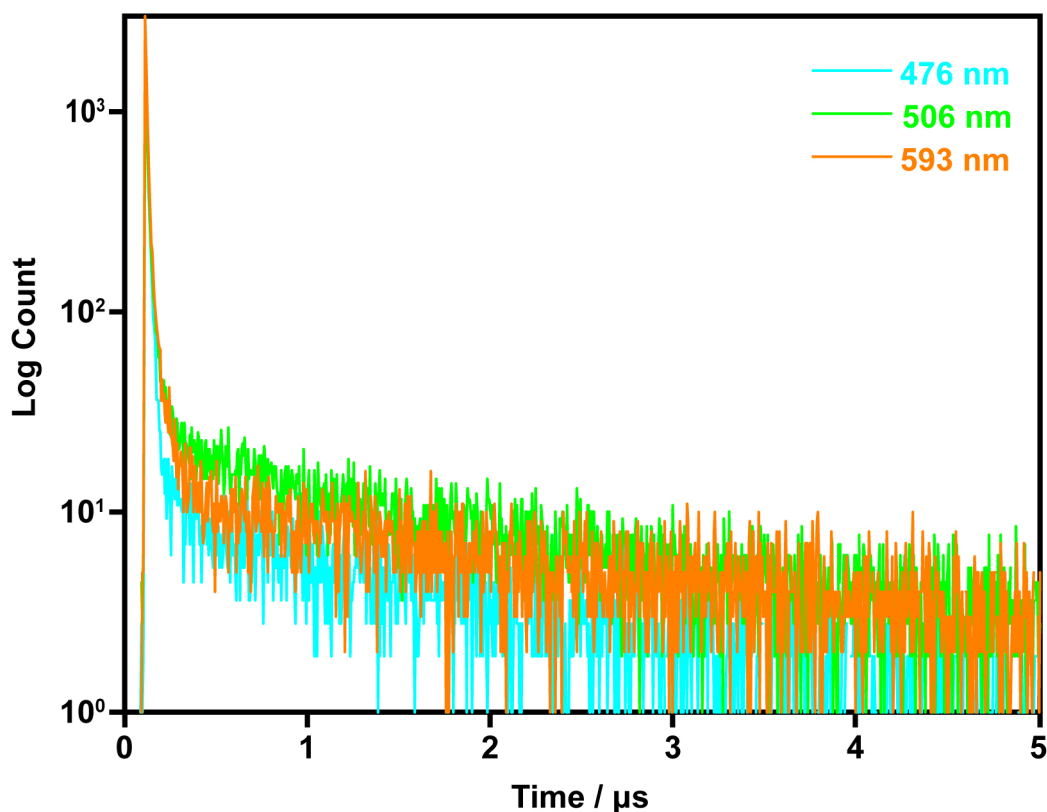


Figure S60. Luminescence lifetime measurement of OGB triblock heterostructure (at 476 nm, 266.41 ns, calculated from three lifetimes which are 11.27 ns with 59% donation and 26.39 ns with 17% donation and 1085.34 ns with 24% donation; at 506 nm, 651.56 ns, calculated from three lifetimes which are 9.95 ns with 36% donation and 38.62 ns with 18% donation and 1404.83 ns with 46% donation; at 593 nm, 456.54 ns, calculated from three lifetimes which are 9.58 ns with 49% donation and 44.66 ns with 22% donation and 1518.33 ns with 29% donation) under an excitation wavelength of 375 nm.

8. Issues on the originality of this work

There have been many studies constructing charge-transfer cocrystals by judicious combination of TCNB as electron acceptors and small-sized molecules as electron donors to achieve color-tunable emission and white-light emitting. In our tasks, we did not claim that we are all the first cases, and we just hoped to provide a comprehensive design scheme towards rainbow/white-light emission in charge-transfer system, which is quite similar to the classic work of three models for the preparation of dye-encapsulated MOFs for white-light emission (J. Am. Chem. Soc. 2019, 141, 14807-14813), although all three models have been reported before. Therefore, we selected eight small-sized electron donors to realize systematic research as much as possible, in order to offer a valuable guidance for future researches. Meanwhile, we tried to make breakthroughs in all the four approaches we present in this work, including the previous reported ones, and eventually we succeeded.

In many previous reports, the bandgap of charge-transfer cocrystal is often approximated as the energy difference between the highest occupied molecular orbital (HOMO) of the donor and the lowest unoccupied molecular orbital (LUMO) of the acceptor. In these works, researchers usually reported the optical properties of two or three charge-transfer cocrystals which show great differences in luminescent

colors between each other. To some extent, such approximation could explain their experimental findings. However, in our work, a series of eight cocrystals with the same acceptor and eight different donors were constructed, providing rich comparative data. This series of results led us to observe some irrationalities of the traditional views, and emphasize the significant role of the photoinduced electron transfer process in charge-transfer systems.

Usually, polymorphs display distinct optical properties. Because the optical properties of most luminescent crystals are caused by the orderly arrangement of molecules in the crystal. However, the origin of the luminescence of charge-transfer cocrystals is the charge transfer between the donor and acceptor, rather than the further packing of charge-transfer pairs in crystals. Therefore, we proposed that the polymorphs of the charge-transfer cocrystals should be served as a suitable platform to realize fine-tuning emissions.

The charge-transfer solid solution can not only realize white light emission in crystal state and solution state, but also present great processing performance. We further fabricate a white light-emitting diode by coating the crystals of charge-transfer solid solution on a 365 nm UV light-emitting diode.

Besides, to the best of our knowledge, we are the first to put forward a novel ABC-type triblock heterostructure based on organic charge-transfer cocrystals.